Provenance of Kalahari Sand: Paleoweathering and recycling in a linked fluvial-aeolian system

Eduardo Garzanti[1*], Guido Pastore[1], Abi Stone[2], Shlomy Vainer[3], Pieter Vermeesch[4], Alberto Resentini[1]

[1] *Laboratory for Provenance Studies, Department of Earth and Environmental Sciences, University of Milano-Bicocca, 20126 Milano, Italy*

[2] *Department of Geography, The University of Manchester, M13 9PL, United Kingdom*

[3] *Institute of Earth Surface Dynamics, University of Lausanne, 1015 Lausanne, Switzerland*

[4] *London Geochronology Centre, Department of Earth Sciences, University College London, London, WC1E 6BT, UK*

Email: eduardo.garzanti@unimib.it (Garzanti), g.pastore2@campus.unimib.it (Pastore), abi.stone@manchester.ac.uk (Stone), shlomy.vainer@mail.huji.ac.il (Vainer), p.vermeesch@ucl.ac.uk (Vermeesch), alberto.resentini@unimib.it (Resentini),

* Corresponding author

Keywords: Kalahari Basin; Sand petrography; Heavy minerals; Detrital-zircon geochronology; Dryland landscape evolution; Drainage changes; Dynamic topography; Sediment-routing connectivity; Southern Africa.

ABSTRACT. We here review what is known about the dunefields and fluvial systems of the Kalahari Basin in terms of geological setting and Quaternary dynamics and set out what has been hypothesized about the provenance of Kalahari sand so far. Previous work has tackled this problem by applying a limited number of techniques (mostly sediment textures and heavy minerals) to parts of the large dryland. The generally highly quartzose mineralogy of aeolian dunes and their compositional variability have been only broadly evaluated and several sedimentological issues have thus remained controversial, including the relative role played by fluvial processes *versus* aeolian reworking of older sediments and weathering controls. This reveals a need for a systematic provenance study that considers the entire basin. For this reason, here we combine original petrographic, heavy-mineral, and detrital-zircon geochronology data with previously published clay-mineral, geochemical, and geochronological information to present the first comprehensive provenance study of the vast Kalahari sand sea.

Our multi-proxy dataset comprises 100 samples, collected across the Kalahari Basin from 11°S (NW Zambia) to 28°S (NW South Africa) and from 15°E (Angola) to 28°30'W (Zimbabwe). Kalahari aeolian-dune sand mostly consists of monocrystalline quartz associated with durable heavy minerals and thus drastically differs from coastal dunefields of Namibia and Angola, which are notably richer in feldspar, lithic grains, and chemically labile clinopyroxene. The western Kalahari dunefield of southeastern Namibia is distinguished by its quartz-rich feldspatho-quartzose sand, indicating partly first-cycle provenance from the Damara Belt and Mesoproterozoic terranes. Within the basin, supply from Proterozoic outcrops is documented locally. Composition varies notably at the western and eastern edges of the sand sea, reflecting partly first-cycle fluvial supply from crystalline basements of Cambrian to Archean age in central Namibia and western Zimbabwe. Basaltic detritus from Jurassic Karoo lavas is dominant in aeolian dunes near Victoria Falls.

Bulk-sediment petrography and geochemistry of northern and central Kalahari pure quartzose sand, together with heavy-mineral and clay-mineral assemblages, indicate extensive recycling via aeolian and ephemeral-fluvial processes in arid climate of sediment strongly weathered during previous

humid climatic stages in subequatorial Africa. Distilled homogenized composition of aeolian-dune sand thus reverberates the echo of paleo-weathering passed on to the present landscape through multiple episodes of fluvial and aeolian recycling.

Intracratonic sag basins such as the Kalahari contain vast amounts of quartz-rich polycyclic sand that may be tapped by rivers eroding backwards during rejuvenation stages associated with rift propagation. Such an event may considerably increase the sediment flux to the ocean, fostering the progradation of river-fed continental-embankments, as documented by augmented accumulation rates coupled with upward increasing mineralogical durability in the post-Tortonian subsurface succession of the Zambezi Delta.

The Central Kalahari is not a true desert. It has none of the naked, shifting sand dunes that typify the Sahara and other great deserts of the world. In some years the rains may exceed twenty — once even forty — inches, awakening a magic green paradise."
Mark Owens, Cry of the Kalahari

1. Introduction

The intracratonic Kalahari sag basin hosts several dunefields that, largely inactive at present, represent the largest sand sea on Earth (Fig. 1). The compositional signatures of such a vast expanse of aeolian sand and their provenance have not been systematically studied so far, and yet encrypted in them lies a bounty of information on the geological, geomorphological, and environmental history of the region. Formed as a consequence of the multistep break-up of Gondwana, the Kalahari Basin presently occupies the core of southern Africa, which experienced dynamic uplift in the Cenozoic and is currently cut across by the southwestward-propagating East African rift system (Haddon and McCarthy, 2005; De Wit, 2007). Complex landscape evolution during the Pleistocene and Holocene was punctuated by a high-frequency alternation of arid and humid climatic stages and consequent repeated changes in hydrology, drainage patterns, and interaction of fluvial and aeolian processes (Burrough et al., 2009a; Hürkamp et al., 2011; Moore et al., 2012; Matmon et al., 2015). Decrypting the Kalahari sedimentary archive is an essential step to improve our understanding not only of the evolution of tropical southern Africa but also of the interplay between tectonic and climatic forces that mould the Earth's surface. Clarifying the control exerted by key climate variables on arid landscapes can, in turn, help test the robustness of numerical models simulating dunefield dynamics and improve model simulations that are used to predict the impact of future climate change on aeolian-dune remobilisation (e.g., Thomas et al., 2005; Mayaud et al., 2007; Vainer et al., 2021a).

This article considers what is known about the Kalahari Basin and its hydrological systems and dunefields (Fig. 2), including an overview of their Quaternary history. The geology of the region is first outlined in the wider context of southern Africa (Fig. 3), before reviewing what was currently known about the provenance of the dunefields and potential fluvial feeder systems. To date, much of the information on provenance has been inferred from likely palaeowind directions (e.g., Thomas, 1987) or by applying a limited number of techniques (mostly sediment textures and heavy minerals) to some parts of this vast basin. Several sedimentological issues have thus remained controversial, including the relative role played by fluvial processes *versus* aeolian reworking and the origin of weathering. Quantitative petrographic data were obtained only on a few aeolian-dune sands in the north and west, and detrital-zircon ages only on fluvial sands in the north (Gärtner et al., 2014; Garzanti et al., 2014a).

For these reasons, we present new results from bulk-petrography, heavy-mineral, and detrital-zircon U–Pb geochronology analyses on 100 aeolian-dune and river-bar sands collected across 17 degrees of latitude from Zambia to South Africa and over 13 degrees of longitude from Angola to Zimbabwe. A set of statistical techniques was applied to this multi-proxy dataset to adequately illustrate the compositional variability of aeolian sand across the Kalahari Basin, reveal meaningful mineralogical patterns, identify the original sediment sources, and gain insight into sand dispersal pathways. In particular, this paper investigates inheritance from past climatic conditions, buffering of environmental signals through linked fluvial and aeolian systems, and progressive compositional homogenization and concentration of most durable minerals acquired through multiple cycles of erosion, transport, deposition, and diagenesis. The new provenance data are integrated and reviewed in terms of what is known about fluvial-aeolian interactions, chemical weathering, and drainage evolution in the Kalahari. Understanding the complexities of sediment transport systems, and particularly how sediment-routing connectivity regulates the transmission of environmental signals from source areas to depositional sinks over spatial and temporal scales, is essential for a realistic interpretation of the stratigraphic record (Romans et al., 2016; Allen, 2017; Caracciolo, 2020).

2. Geology of southern Africa

Southern Africa was amalgamated through multiple tectono-magmatic events dating back to the Archean and culminated with the Neoproterozoic Pan-African orogeny (Fig. 3; Hanson, 2003). The Archean core consists of the Kaapvaal and Zimbabwe Cratons, welded by the Limpopo Belt. The Kaapvaal Craton, progressively amalgamated between 3.7 and 2.7 Ga, was stabilized by 2.6 Ga, and eventually intruded by the Bushveld Complex at 2.06 Ga (Eglington and Armstrong, 2004). The Zimbabwe Craton, comprising 3.5-2.95 Ga gneisses non-conformably overlain by volcanic and sedimentary rocks and 2.7 Ga greenstone belts, was eventually sealed by the Great Dyke Swarm at ~2.6 Ga (Kusky, 1998; Jelsma and Dirks, 2002). The ~200 km-wide Limpopo Belt includes high-grade orthogneisses, retrograde amphibolite-facies metasedimentarary rocks, and granitoids with ages clustering at 3.3-3.2, 2.7-2.6, and 2.1-2.0 Ga (Zeh et al., 2007).

This composite Archean core grew progressively during Proterozoic orogenic cycles that generated the discontinuously exposed mid-Paleoproterozoic Magondi-Okwa-Kheis Belt in the west and the latest Mesoproterozoic Namaqua–Natal Belt in the south. In the northwest, the Angola Block represents instead the southern part of the Congo Craton, cored by largely mid-Paleoproterozoic (~2 Ga) mid-crustal granitoid gneisses (De Carvalho et al., 2000; McCourt et al., 2013; Jelsma et al., 2018).

Stabilization of the Proto-Kalahari Craton by 1.75 Ga was followed by intraplate magmatism at 1.4-1.35 Ga and again at 1.1 Ga (Hanson et al., 2006). Amalgamation of the Kalahari Craton was completed by 1.0 Ga (Jacobs et al., 2008), when the Namaqua–Natal Belt was generated by arc accretion and continental collision. This orogen extends from SW Namibia to NE South Africa and includes Paleoproterozoic basement and up to high-grade metasedimentary rocks intruded by voluminous granitoids dated at 1.2-1.0 Ga (Eglington, 2006). The Mesoproterozoic volcano-sedimentary Sinclair Group of southern Namibia underwent only low-grade deformation and was intruded by numerous granitoids (Becker et al., 2006).

Cratonic southern Africa was finally welded to the Congo Craton in the north during the major Neoproterozoic Pan-African orogeny, testified by the Damara–Lufilian–Zambezi Belt stretching from coastal Namibia in the west and across Botswana and southern Zambia to connect with the Mozambique Belt in the east (Frimmel et al., 2011; Goscombe et al., 2020). The Damara Belt in Namibia includes 2.0-1.2 Ga basement gneisses overlain by Neoproterozoic metasediments intruded by 570-460 Ma granitoids (Miller, 2008). A 3 km-thick succession of Neoproterozoic to Cambrian sandstone, mudrock and limestone was deposited in the foreland of the Damara Orogen in southern Namibia (Nama Group; Blanco et al., 2011). The Lufilian Arc consists of metasedimentary and metaigneous rocks hosting Cu-Co-U and Pb-Zn mineralizations (Kampunzu and Cailteux, 1999; Eglinger et al. 2016). The Zambezi Belt contains a volcano-sedimentary succession deformed under amphibolite-facies conditions at 0.9–0.8 Ga (Hanson 2003), whereas eclogite-facies metamorphism dated as 592 Ma constrains the timing of subduction and thrust emplacement as 550-530 Ma (Hargrove et al., 2003; John et al., 2004).

Initial disruption of the Gondwana supercontinent was recorded by the several km-thick Upper Carboniferous to Lower Jurassic Karoo Supergroup, covering almost two-thirds of southern Africa. Basin subsidence in the southern retroarc basin was induced by subduction of paleo-Pacific lithosphere, while transtensional stress propagated southwards from the Neotethyan rift in the north (Catuneanu et al., 2005). The Karoo succession begins with diamictite, turbidite, and coal-bearing fluvio-deltaic strata, followed by braidplain sandstone, mudrock, and aeolian sandstone (Johnson et al., 1996). Permian sandstones contain andesitic-dacitic volcanic detritus (Johnson, 1991) and interlayered tuffs yielding ages mainly between 270 and 260 Ma (Lanci et al., 2013; McKay et al., 2016). Karoo sedimentation was terminated by flood-basalt eruptions recorded throughout southern Africa around 183 Ma (Svensen et al., 2012; Greber et al., 2020). A vast network of dolerite dykes and sills suggests that tholeiitic lavas originally covered an area of ~2.5 million km^2.

The passive margins surrounding Africa developed after rifting of the Indian and Atlantic Oceans in the Late Jurassic and Early Cretaceous, respectively. Widespread intrusion of pipe-like bodies, including diamond-bearing kimberlites, took place in the Cretaceous to Paleogene (Moore et al., 2008).

In the Kalahari Basin, stretching ~2200 km in the hinterland from the Congo to South Africa, up to 450 m-thick sediments were deposited since the Late Cretaceous (Haddon and McCarthy, 2005). The Plio-Pleistocene consists of gravel, clay, and aeolian sand with calcrete and silcrete (Thomas and Shaw, 1990; Vainer et al., 2018a). In the Quaternary, the East African rift propagated along a network of unconnected basins extending from Lake Tanganyika to the Okavango Graben and central Namibia farther west (Modisi et al., 2000; Kinabo et al., 2007; Vainer et al., 2021b).

3. The Kalahari Basin

The intracratonic Kalahari sag basin comprises the largest continuous sand sea on Earth, which extends for over 2.5 x 10^6 km^2 (Fig. 1). The interior of the Kalahari is an elevated plateau with flat topography (average altitude 1200 m), delimited by relatively steep escarpments down to the Atlantic Ocean in the west and to the Indian Ocean in the east. Kalahari Group sediments — including basal gravel and conglomerate, sandstone with calcrete, and unconsolidated sand — stretch north from the Orange River in South Africa (~29°S) to the Democratic Republic of Congo (~6°S; Haddon and McCarthy, 2005).

The landscape across the Kalahari is varied, encompassing spatially discrete dunefields dominated by linear dunes, the Okavango alluvial fan (delta) and wetlands in northern Botswana, and aligned drainage and pans (Lancaster, 1981; Thomas and Shaw, 1991; Shaw and Goudie, 2002; Goudie and Viles, 2015). The erg is traversed by rivers that were initially mostly endorheic but were progressively captured from both sides by rivers eroding headwards from the coast (e.g., Moore and Larkin, 2001). Development of endorheic drainage and expansion of a landlocked sand sea in this arid tropical region was favored by multiple phases of tectonic activity in bordering areas since the Mesozoic, promoted by asthenosphere upwelling during the rifting stage and maintained during the passive-margin stage by flexuring associated with sediment loading of the continental terrace, or rejuvenated by isostatic processes or buoyancy forces in the mantle (Moucha and Forte, 2011; Blenkinsop and Moore, 2013).

3.1. Climate

Climate in southern Africa results from the disturbance by a great land mass of quasi-stationary anticyclones over the Atlantic and Indian Oceans, corresponding to the descending limb of the Hadley Cell (Schulze, 1972). A major influence is exerted by the Intertropical Convergence Zone and associated Tropical Rain Belt (Nikulin and Hewitson, 2019), by the Congo Air Boundary, and by temperate frontal systems within the southern hemisphere westerlies in the west and south. The Indian Ocean is a major source of water vapor for the sub-continent via easterly winds (Fig. 2A), and climatic changes within southern Africa have been linked to the variability of Indian Ocean surface temperature (Partridge, 1993; Tyson and Preston-Whyte, 2000; Washington and Preston, 2006; Vigaud et al, 2009). The South Indian Convergence Zone may extend its influence on the sub-continent via synoptic systems known as Tropical Temperate Troughs, which connect the mid-latitudes to the tropics (Cook, 2000; Todd et al., 2002).

Oceanic currents also affect climate in the continental interiors (Walker, 1990). The warm Agulhas current flows southward along the coast of Mozambique (Fig. 2C) , allowing humid air masses to enter the continent from the Indian Ocean, thus causing heavy rains onto orographic barriers (e.g. Drakensberg Mountains of Lesotho) and a marked westward decrease in precipitation across southern Africa (Reason, 2001) (Fig. 2B, 2C). The Agulhas current is retro-deflected at 16-20°E longitude when encountering the cold Benguela current (Lutjeharms and Van Ballegooyen, 1988), which displaces Antarctic water along the Atlantic coast of South Africa, Namibia and southern Angola, causing low sea-surface temperatures, low humidity of southerly winds, and very little rain through the year (Rogers and Bremner, 1991).

Rainfall occurs mainly during winter in the southwestern corner of the sub-continent and during summer in the rest of the region. The aridity center is situated in southern Botswana. Annual rainfall increases from 150 mm in the southwest to 400 mm in Zimbabwe, and climate becomes sub-humid and less seasonal northward (Fig. 2B, 2C).

The wind regime in the Kalahari is more complex than expected in areas of linear dune development (Fig. 2A), being influenced by the seasonal fluctuation of the high-pressure cells (Tyson and Preston-Whyte, 2000). The dry winter season is characterized by southeasterly winds associated with the South Atlantic anticyclone (Bultot and Griffith, 1972). In the summer, winds blow mainly from the north in the eastern Kalahari and from the west in the western Kalahari (Nicholson, 1996). The southwestern Kalahari is dominated by southwesterly winds (Wiggs et al. 1996).

3.2. Hydrology

Three major rivers flow from humid Angola and western Zambia across the northern Kalahari: the Cunene, the Okavango, and the Zambezi (Fig. 1). The Cunene, sourced in Angolan highlands uplifted in the Plio-Quaternary (Klöcking et al., 2020; Vainer et al., 2021b), runs along the westernmost edge of the sand sea drained by the Caculuvar and Mucope tributaries (Fig. 1A; Shaw and Goudie, 2002). Once endorheic and emptying into what is today Etosha Pan (Miller et al., 2010), the Cunene was captured by a headward eroding coastal stream and its youthful terminal tract now debouches into the Atlantic Ocean (Goudie and Viles, 2015 p.14-15).

The Okavango, the main endorheic river of the Kalahari, is fed from humid Angola, where the southward migration of the Congo Air Boundary brings heavy rains between December and March (annual rainfall ≤1400 mm). The flood-wave takes until August to filter through the anastomosing channels and swamps of the Okavango, the largest wetland in southern Africa and the largest inland delta on Earth (McCarthy and Ellery, 1998). Suspended sediments supplied annually to the Okavango Delta amount to only ~19% of total load (McCarthy et al., 2012), suggesting that weathering intensity is presently quite low even in the northern Kalahari Basin. Sedimentation of fine sand dominates the upper delta, whereas chemical sedimentation in the form of calcrete and silcrete prevails in the lower delta (McCarthy and Metcalfe, 1990). Finally reunited in the Boteti River, the drastically reduced flood waters traverse another stretch of the Kalahari, ending endorheically in the Makgadikgadi Pan. The main source of water for the pan is the ephemeral Nata River, sourced in Zimbabwe to the east.

The Zambezi and its major Cuando tributary (named Kwando, Linyanti, and next Chobe after entering the Okavango Graben in the Caprivi strip) also flow across the northern Kalahari. Downstream of Victoria Falls, the Zambezi plunges into deep gorges carved in Karoo basalt, heading towards the Indian Ocean (Moore et al., 2007). The Gwai River drains the eastern edge of the sand sea in Zimbabwe, along with its tributaries once directed westwards toward the central Kalahari (Thomas and Shaw, 1988).

In Namibia, three ephemeral rivers draining into the Kalahari flow only in case of exceptionally heavy and continuous precipitation. The Omatako in the north is an Okavango tributary, the Rietfontein dries up in central Botswana as a former tributary of the fossil Okwa River (Fig. 2A), and the Nossob in the south joins the Molopo River. The occasional floods in the Nossob and Molopo are absorbed along the way and recharge groundwater aquifers with water losses up to 90% and 80%, respectively (van Veelen et al., 2009). The flow of the Nossob and Auob (its major western tributary) typically ceases between 24°S and 25°S, respectively, and the Molopo seldom flows west of 23°40’E (Nash, 2015). The Molopo has continuous river flow and reaches the Orange River — thus becoming exorheic — only during extreme events, which have a return period of between 20 and 50 years (Nash and Endfield, 2002). The Kuruman, the major Molopo tributary in South Africa, is also dry except for flash floods, but has permanent flow over its first 10 km owing to its famous dolomite spring source (*Die Oog*, the ‘Eye of the Kalahari’), which has yielded a constant ~750 m^3/hour flux during the last two centuries at least (Shaw et al., 1992).

The southern and western Kalahari rivers are misfit streams within wider, flat-bottomed channels reaching 0.5 to 1.8 km in width (Bullard and Nash, 2000). They contain gorge-like sections with varying steepness (typical incision depth ~25 m) and show evidence of groundwater processes (sapping and deep weathering; Shaw and deVries, 1988; Bullard and Nash, 1998; Stone, 2021a).

Pans (endorheic basins that temporarily host water and deposit mostly salt and clay) are widespread in the Kalahari, found in depressed areas where an integrated fluvial system is lacking and surface geology is suitable (soluble duricrusts or regions with deflatable loose silt and sand). They occur in many interdune corridors of the linear dunefields and in higher concentration along the western watershed of the southern dunefield (Goudie and Thomas, 1985; Lancaster, 1986; Lancaster, 1978).

3.3. Dunefields

The five dunefields identified in the Kalahari Basin (NWK, northwestern; NEK, northeastern; EK, eastern; WK, western; SK southern; Fig. 2A) are all dominated by linear dunes (Thomas and Shaw, 1991; Shaw and Goudie, 2002). Other morphologies include topographically constrained dunes occurring at hill and mountain fronts (Tyson, 1999) and lunette dunes fringing the widespread pans (Telfer and Thomas, 2006; Hürkamp et al., 2011). There are also areas with sand sheets (e.g., southwestern Kalahari; Bateman et al., 2003) and areas of degraded dune patterns resembling barchanoid ridges on the eastern edge of the western Kalahari near the Botswana/Namibia border (McFarlane et al., 2005; Stone, 2021a).

Kalahari dunefields may have started to accumulate in the early Pleistocene (Partridge, 1993; Miller, 2014; Vainer et al., 2021a). In the western Kalahari, dunes superimposed over a megafan are inferred to be younger than the 4-Ma-old mainly vertebrate fossils that lie below the sand (Miller, 2008; Miller et al., 2010), whereas dunes in the east lie below Middle Stone Age artifacts, constraining the youngest possible age for sand deposition as > 200 ka (McFarlane and Segadika, 2001). In the southern Kalahari, Vainer et al. (2018b) simulated a range of scenarios of sand exposure and burial based on cosmogenic nuclides and luminescence constraints and suggested there may have been 22 overturning cycles since sand was available for aeolian distribution, at 1.5-2.2 Ma and/or 4.2-5.2 Ma (in agreement with Miller, 2014).

Reworking of the initially produced sand occurred throughout the Quaternary, and burial ages for the most recent of any dune recycling and accumulation episodes are determined by luminescence dating (see compilation spanning ~190 ka for the INQUA Dune Atlas by Thomas and Burrough, 2016). Finite luminescence ages for basal sediments of linear dunes range from 1.1±0.1 ka to 104±8 ka (including samples in saturation, i.e., at the upper limit of the dating technique that can be extended if integrated with cosmogenic-nuclide dating; Vainer and Ben Dor, 2021).

Today, precipitation levels, vegetation cover, and insufficient wind energy hamper aeolian activity even in the driest area of the erg, excepting some blowing sand on dune crests in the western and southern Kalahari (Wiggs et al., 1995; Bhattachan et al., 2013). The cover of grasses and savannah bush increases on a broad north-south gradient, with increasing concentrations of woodland north of ~21ºS (Van Rensburg, 1971; Thomas and Shaw, 1991). Therefore, Kalahari dunes are currently largely inactive, sometimes pedogenically modified and in places extensively degraded, with a higher proportion of silt and clay than normally found in active dune fields (Thomas, 1984; Wiggs et al. 1995; McFarlane et al., 2005). The extent of this alteration by slope and locally tectonic processes (McFarlane and Eckardt, 2007) increases northwards and eastwards as the woodland vegetation cover increases, and in western Zambia eroded dune crests largely stabilized by vegetation may rise only ~5 m from the vegetated interdunes (O'Connor and Thomas, 1999).

The trend of linear dunes changes from ESE/WNW to E/W and then to ENE/WSW from west to east in the northern Kalahari (NWK, NEK, and EK), it is NE/SW south of Makgadikgadi and NW/SE to NNW/SSE in the southern Kalahari (WK and SK) (Fig. 2A). These patterns have been ascribed to wind circulation around, and shifts in the position of, the southern African anticyclone (Lancaster, 1979, 1981; Thomas, 1984). However, the accompanying idea that there were discrete periods of formation for each dunefield has been overturned by the large number of compiled luminescence ages, indicating multiple accumulation phases in each region over the last ~190 ka.

Five different classes of linear dunes are identified in the southern Kalahari (WK, SK; Bullard et al., 1995; Bullard and Nash, 1998): 1) simple and discontinuous; 2) simple and continuous; 3) compound with common Y-junction branches; 4) compound with more-obtuse angles between branches; 5) no preferred orientation and discontinuous. The tallest and most closely spaced dunes are found in the southeast of this region, as shown by detailed morphometric analysis using ASTER global digital-elevation-model data (White et al., 2015). This contradicts the often-reported relationship of bigger dunes with wider spacing, suggesting that these dunes have experienced a reduction in sediment supply through time and/or post-depositional modification (Kiss et al., 2009; White et al., 2015).

3.4. Duricrusts

Duricrusts that act as cement and stabilize sand's potential movement are widespread below, within, and above Kalahari sands, covering most of the surface in the southern part of the basin (Botha, 2000). Studies based on their minerology, micromorphology, bulk geochemistry, isotopic signature, chronology, and geomorphological context have suggested several formation mechanisms dependent on hydrology and climate. Semi-arid to arid conditions under alternating dry and humid stages are generally considered as suitable for their precipitation (Kampunzu et al., 2007; Ringrose et al., 2009), but their paleoenvironmental interpretation is not straightforward (Summerfield, 1983; Nash and McLaren, 2003).

Duricrusts are chemical precipitates that form under saturation of the host sediment through a combination of lateral and vertical transfer mechanisms. Therefore, they are not restricted to one phase within a chronological stratigraphy and occur in both vadose and phreatic environments. Alternating conditions (e.g., moisture availability, temperature, vegetation) promote changes in pH that commonly result in mixed compositions of cements, which range from pure carbonate to pure silica and may include Fe-oxy-hydroxides and clays (Shaw and Nash, 1998; Nash et al., 2004; Kampunzu et al., 2007; Vainer et al., 2018b). Multi-phase accumulation through repeated dissolution and re-precipitation occurs at varied subsurface and surficial settings, including paleolakes, pans, and marginal pools (McCarthy and Ellery, 1995; Ringrose et al., 2002; Thomas et al., 2003), valley-fills (Nash and McLaren, 2003), and pedogenic profiles (Watts, 1980), where flora and fauna may be involved in their generation.

Varied formation settings and processes, with consequently diverse textures ranging from dispersed powder to nodular and hardpan, has led to different classification criteria (Goudie, 2020). These include geomorphological and hydrological conditions as well as macro- and micromorphological characteristics (size, structure, mineralogy, porosity, biological components, secondary filling and coating) and chronological relationships between the precipitating phases (Nash and Shaw, 1998; Nash and McLaren, 2003).

In the Kalahari, indurated layered carbonate characterizes weathering profiles in NW Botswana and could be widespread throughout the basin but covered by unconsolidated sand (McFarlane et al., 2010). Based on Sr isotopic ratios, chemical precipitation is inferred to have occurred from solutions migrating laterally from dolomitic rocks when aquifer levels dropped shortly after clastic deposition (Vainer et al., 2018b). A source other than underlying bedrock for the cementing agents was similarly inferred for duricrusts in southern and central Botswana based on geochemical differences with the underlying bedrock (Nash et al., 2004).

U-Pb dating of carbonates deposited in a mega-fan environment in the Etosha sub-basin reaches back to the early Eocene (Houben et al., 2020), much earlier than the establishment of dunefields in the Kalahari. Because of intrinsic difficulties in radiometric dating of calcrete (Geyh and Eitel, 1997), the age of duricrusts is mainly constrained by the association with fossils and artefacts, indicating formation since the early Pleistocene and throughout the Quaternary (Haddon, 2005). Over the last decades, luminescence dating has allowed to establish when quartz grains within calcrete were last exposed to light, confirming duricrust formation spanning at least from the middle and late Pleistocene (Ringrose et al., 2002) to the Holocene (Burrough et al., 2009a).

3.5. Quaternary climate change

In the Kalahari dryland, Quaternary environmental and climatic changes are documented by different proxies in a range of archives, including aeolian sand dunes, former lake shorelines, pan deposits and fringing lunette dunes, fluvial sediments, tufa carbonates, speleothems, groundwater and rock shelter deposits (animal and human middens and rock art) (table 1 in Stone, 2021b). The Quaternary dynamics of aeolian-fluvial interactions can be put into context by combining these different archives. Given the size and current climatic heterogeneity of the Kalahari Basin it is pragmatic to consider three broad sub-regions: i) northern (including the NWK, NEK and EK dunefields); ii) southern (including the WK and SK dunefields); iii) eastern, with no major dunefield.

Over the past ~150 ka, at least seven wetter intervals are identified in these sub-regions, which are not paced consistently with precession and whose onset and end do not align with global marine oxygen isotope stages. Some appear to be widespread, but others display opposing meridional trends. Data compiled from the INQUA Dune Atlas by Thomas and Burrough (2016) indicate relatively continuous aeolian-dune accumulation across most of the Kalahari over the past 190 ka, with only a few gaps (174-107 ka, 96-87 ka, and 38-42 ka) possibly ascribed to a lack of preservation. The implication of this dataset of ~400 ages is that the pattern of episodic aeolian-dune formation and aridity proposed by Stokes et al. (1998) is an artefact driven by low sampling density across space and to only shallow depths within a dynamic and heterogeneous landscape (Stone and Thomas, 2008).

A first wetter interval at ~140 to 120 ka is seen in the northern sub-region, when diverse isolated basins became interconnected in mega-lake Makgadikgadi reflecting changed hydroclimatic conditions in humid Angola (Burrough et al., 2009b). Speleothem growth reflects instead more localised climate conditions (133±27 ka; Brook et al., 1998). In the southern sub-region, presence of palygorskite suggests semi-arid climate from 156±11 to 121±6 ka (Lukich et al., 2019; 2020). In the southern Kalahari, the only preserved evidence of linear-dune accumulation between ~174 and 107 ka is a mottled sandstone unit dated by luminescence as between 160 and 108 ka (Bateman et al., 2003).

A second wetter interval between ~112 and 90 ka is recorded by mega-lake Makgadikgadi phases (105±4 ka and 92±2 ka; Burrough et al., 2009b) and speleothem growth (112±5 to 108±7 ka and

93±6 ka: Brook et al., 1998). Evidence for aeolian-dune accumulation is lacking in the southern sub-region during this period, when there was locally abundant re-surging groundwater (111±3 to 102±2 ka; Wilkins et al., 2021) and increased moisture availability at Kathu Pan (Lukich et al., 2020).

A third wetter interval is recorded between ~80 and 70 ka at Etosha Pan (Hipondoka et al., 2014) but not in the mega-lake Makgadikgadi system, whereas semi-arid conditions are recorded at 74±5 ka in the south at Kathu Pan (Lukich et al., 2020). In contrast, a fourth interval is documented between ~63 and 43 ka by a mega-lake Makgadikgadi phase at 64±2 ka, and by speleothem growth (~61 ka; Brook et al., 1998; ~51-43, Holmgren et al., 1995; 58-46 ka, Holzkämper et al., 2009; from 56.8±0.4 to 43±7 ka, Pickering et al., 2007). The southern sub-region recorded semi-arid conditions at 55±3 ka (Lukich et al., 2020) and aeolian dunes continued to accumulate (Thomas and Burrough, 2016). A following drier interval is documented in the eastern sub-region by a lack of speleothem growth between ~43 and 27 ka (Holmgren et al., 1995) and groundwater record (Kulongski et al., 2004). However, wetter conditions are testified between ~43 and 30 cal ka B.P. in the western part of the southern Kalahari (Schüller et al., 2018). Aeolian dunes accumulated consistently, suggesting sufficient windiness and perhaps inadequate moisture availability to keep vegetation cover below a limiting threshold.

A fifth wetter interval is documented in the northern sub-region at 39±2 ka and 27±1 ka by two mega-lake Makgadikgadi phases (Burrough et al., 2009) and at 36-32 and 27-22 ka (Thomas et al., 2003). Evidence includes aquifer recharge at ~36-33 ka (Stute and Talma, 1998), speleothem growth at ~33 ka (Brook et al., 2010), and pan-floor flooding at 32±5 ka (Telfer et al., 2009). In contrast, dry conditions are documented in the southern sub-region (~30-25 cal ka B.P.; Schüller et al., 2018), where aeolian dunes continued to accumulate (Thomas and Burrough, 2016). Wetter conditions started later in the eastern sub-region, as indicated by speleothem growth from 27-21 ka (Holmgren et al., 1995), 24.3-12.7 ka (Holmgren et al., 2003), and 16.5±0.2 ka (Pickering et al., 2007).

A sixth wetter interval is documented between ~23 and 16 ka as a mega-lake Makgadikgadi phase (17±2 ka; Burrough et al., 2009b) and as lake phases at Etosha Pan (23-21 and 18-16 ka; Hipondoka et al., 2014). In the southern sub-region, fluvial units were dated at 23 ka and 18 ka in the lower Molopo basin (Hürkamp et al., 2011), pan flooding at ~20 ka (Telfer et al., 2009), and speleothem growth at 32-17 ka (Brook et al., 2010). In contrast, drier conditions are indicated at 22±1 ka by a hardpan unit at Kathu Pan indicating a strongly negative moisture balance (Lukich et al., 2020), but wet enough at the eastern fringes of the Kalahari for speleothem growth through to 21 ka (Holmgren et al., 1995).

A seventh wetter interval is recorded in the northern sub-region at 16-12 ka (Thomas et al., 2003) and in the southern sub-region at 15-13 cal ka B.P. (Schüller et al., 2018). This episode is not documented in the mega-lake Makgadikgadi system and aeolian dunes continued to accumulate in the southern sub-region (Thomas and Burrough, 2016).

At the start of the Holocene, wetter conditions are indicated by a mega-lake Makgadikgadi phase at 8±5 ka (Burrough et al., 2009b), by an Etosha Pan lake phase at ~10 ka (Hipondoka et al., 2014), and by speleothem growth at ~8.2 ka (Brook et al., 1998), consistently with an absence of age evidence for aeolian-dune activity since ~8 ka in the northeastern Kalahari (Thomas and Burrough, 2016). In contrast, only episodic flash-flood events are documented in the lower Molopo from ~9.5 to 6.5 ka (Schüller et al., 2018) and aeolian dunes were active in the southern-sub-region during this time (Thomas and Burrough, 2016). Speleothem growth ceased before the Holocene in the eastern sub-region (Holmgren et al., 1995) but continued from ~ 5 ka onwards in the north (Brook et al., 1998). A wet phase is recorded at ~5.5 cal ka B.P. in the south (Schüller et al., 2018), whilst aeolian-dune activity continued in the southern sub-region (Thomas and Burrough, 2016). Overall, the spacing of wetter intervals does not demonstrate a regular periodicity, suggesting an interplay of factors more complex than solely global glacial-interglacial cycles or precession-paced forcing of hydroclimate.

4. Overview of previous work on the provenance of Kalahari sands

The provenance of Kalahari sands has not been investigated thoroughly by a multi-technique approach so far. Previous surveys recognized the highly quartzose composition of aeolian sands, but their compositional variability has been only broadly evaluated, and the origin of Kalahari dunefields was mostly ascribed to either reworking of older sediments (e.g., Du Toit, 1954; Baillieul, 1975; Thomas, 1987) or dominant fluvial processes (e.g., De Ploey et al., 1968; Verboom, 1974; Moore and Dingle, 1998). Petrographic, mineralogical, geochemical, and geochronological results from aeolian and river sediments collected in the Kalahari Basin and illustrated in Garzanti et al. (2014a, 2014b) complement the new dataset obtained in this study and will be summarized and discussed later on.

The earliest heavy-mineral study of Kalahari sands was carried out by Poldervaart (1957), who identified tourmaline as a ubiquitous component, associated with zircon increasing eastwards at the expense of staurolite and kyanite. In his survey across Botswana, Baillieul (1975) distinguished four different types of Kalahari sands according to their texture, composition, and origin: 1) pure quartz sand reworked from older longitudinal dunes in northwestern Botswana; 2) finer-grained feldspar-bearing sand largely derived from recycling of the feldspatho-quartzose Neoproterozoic Ghanzi Sandstone in central-western Botswana; 3) pure quartz sand inferred to be recycled from Upper Triassic/Lower Jurassic sandstones of the Karoo Supergroup in central to southwestern Botswana (Boocock & Van Straaten, 1962); 4) various sands of fluvial origin in eastern Botswana, locally containing micas or basaltic rock fragments and largely derived from diverse exposed bedrocks. Thomas (1987) emphasized the remarkable homogeneity of textural and compositional features, held to testify an overriding importance of aeolian activity across the Kalahari.

In their textural and mineralogical study of the Kalahari Erg in NW South Africa, central Botswana and NE Namibia, Schlegel et al. (1989) distinguished between sand collected from the crest of modern aeolian dunes and 'mixed sands' collected in interdune areas or close to ephemeral rivers or pans. They found that tourmaline and staurolite are most abundant in dune-crest samples, whereas garnet, zircon, amphibole, pyroxene, rutile, sillimanite, andalusite, and opaque oxides (magnetite, ilmenite, and hematite) are more abundant in the 'mixed' samples. In South Africa, aeolian sand resulted to yield subrounded to very well-rounded tourmaline, staurolite, kyanite, and opaque oxides. In Botswana and Namibia, more heterogeneous suites consist of mostly well-rounded tourmaline with subordinate staurolite, epidote, and zircon. Heavy minerals were observed to be denser, less spherical and less rounded in 'mixed samples', garnet commonly occurring as broken angular fragments. Main source rocks were held to be Nama and Karoo Group siliciclastics in South Africa and Botswana.

In their textural and mineralogical study of central Botswana cover sands, Moore and Dingle (1998) failed to find a correspondence between the variability of sediment textures and wind patterns, and thus inferred a dominance by fluvial processes. Ephemeral streams and sheetwash were inferred to produce heavy-mineral enrichment in coarser proximal sands passing to finer sediments with fewer heavy minerals in distal settings. Tourmaline (mainly in the southwest), staurolite (mainly in the north), and kyanite were confirmed as the most common heavy minerals.

More recently, Haddon and McCarthy (2005) recognized the major role played by both fluvial and aeolian processes and identified local reworking from older deposits as a major source of Kalahari sand. In a most recent study, Vainer et al. (2018a) used detrital mineralogy, elemental geochemistry, and Sr, Nd and Pb isotopic ratios to detect provenance changes through a complete Quaternary section of Kalahari Group sediments in South Africa. Provenance from distant Angolan highlands *via* a trans-Kalahari palaeodrainage system was inferred for the basal part of the section, overlain by strata containing detritus derived locally from volcano-sedimentary rocks of the Archean Kaapvaal Craton exposed in the east and south. The more recent aeolian sands indicated instead sediment supply from Paleoproterozoic source rocks in the west and northwest. Chemical proxies suggested that weathering intensity was typical of humid areas for the basal part of the section at a time of relatively dense hominin occupation of the area, but limited to groundwater alteration and precipitation of duricrusts in the overlying strata.

Based on geochemical data, sediments of the Okavango Basin were considered to represent a mixture of detritus derived from Proterozoic basement rocks exposed in Angola, Namibia, and NW Botswana with locally recycled aeolian sand and calcareous soils (Huntsman-Mapila et al., 2005). Using elemental geochemistry complemented by Nd, Sr, and Pb isotopes, Vainer et al. (2021b) outlined a more complex provenance pattern, with detritus derived from multiple sources including the Angola Shield in the northwest, the Archean Kasai Craton in the north, Mesoproterozoic granitoids of the Choma-Koloma Block in the east, and the Ghanzi-Chobe and Damara Belts in the west, with possible contribution also from the Lufilian Belt and Karoo basalts.

Gärtner et al. (2014) used U-Pb detrital-zircon geochronology and zircon morphology from sand carried by the Cunene, Okavango, Cuando, and uppermost Zambezi Rivers to pinpoint the protosources of sediment recycled from and fed into the northern Kalahari Basin. They suggested that most sediment originated from the Lufilian and Kibaran Belts with westward increasing input from the Damara Belt. Zircons derived from the Angola Block were detected only in the Cunene and westernmost part of the Okavango drainage basins.

5. Methods

In this provenance study, we have analysed 57 samples of aeolian dunes collected across the vast Kalahari sand sea in the frame of diverse research projects (Stone and Thomas, 2008; Matmon et al., 2018; Burrough et al., 2019; Stone et al., 2019; Wittman et al., 2020; Vainer et al., 2021a). Another 43 sand samples collected from exposed sandbars or dry riverbeds in Angola, Botswana, Zambia, Zimbabwe, Namibia and South Africa, and previously studied with similar and complementary methodological approaches (Garzanti et al., 2014a, 2018a, 2021a), were considered to monitor changes in sediment composition associated with fluvial-aeolian interactions. Aeolian-dune samples are mostly fine to lower medium sand (average 2.3±0.5 ϕ), whereas river sands range more widely from fine to coarse (average 1.8±0.8 ϕ). Full information on sampling sites is provided in Appendix Table A1 and Google Earth™ file Kalahari.kmz.

5.1. Petrography

Petrographic composition of each sand sample was determined by counting ≥ 400 points in thin section by the Gazzi-Dickinson method (Ingersoll et al., 1984). Sands are classified by their main components exceeding 10%(Q+F+L) (e.g., in a feldspatho-quartzose sand Q > F > 10%(Q+F+L) > L). Among feldspatho-quartzose sands, feldspar-rich (Q/F < 2) and quartz-rich (Q/F > 4) compositions are distinguished; pure quartzose sand has Q > 95%(Q+F+L) (Garzanti, 2019). Cross-hatched microcline is called for simplicity microcline*. Rock fragments were classified by protolith composition and metamorphic rank (Garzanti and Vezzoli, 2003). The complete petrographic dataset is provided in Appendix Table A2.

5.2. Transparent heavy minerals

From the bulk sample or from a wide size-range obtained by wet sieving, heavy minerals were separated by centrifuging in Na-polytungstate (2.90 g/cm^3) and recovered after partial freezing of the test tube with liquid nitrogen. The dense fraction thus obtained was weighed, split with a micro-riffle box, and mounted on a glass slide with Canada balsam for counting. About 200 to 250 transparent heavy minerals were either counted by the area method or point-counted at suitable regular spacing to obtain real volume percentages (Galehouse, 1971). Well sorted samples (19 aeolian dunes and 8 fluvial bars) were analysed in bulk. For moderately to poorly sorted samples, where the co-existence of detrital minerals with widely different sizes makes mounting and identification difficult (Mange and Maurer, 1992), we analyzed size windows ranging in width from at least 3.5 ϕ (32-355 μm) to 5 ϕ (15-500 μm) or more (e.g., >15 μm or > 32 μm).

Transparent-heavy-mineral concentration (tHMC; Garzanti and Andò, 2007, 2019) ranges from extremely poor (tHMC < 0.1), very poor (0.1 ≤ tHMC < 0.5), poor (0.5 ≤ tHMC < 1) and moderately poor (1 ≤ tHMC < 2), to moderately rich (2 ≤ tHMC < 5), rich (5 ≤ tHMC < 10), very rich (10 ≤ tHMC < 20), and extremely rich (20 ≤ tHMC < 50). The sum of the percentages of zircon, tourmaline, and rutile (collectively called ZTR minerals throughout the text) expresses the mineralogical durability of the suite (ZTR index of Hubert, 1962; Garzanti, 2017). The "Amphibole Color Index" ACI varies from 0 in detritus from upper-greenschist/lower-amphibolite-facies metamorphic rocks yielding exclusively blue/green amphibole to 100 in detritus from granulite-facies or volcanic rocks yielding exclusively brown amphibole or oxyhornblende (Andò et al., 2014). Transparent-heavy-mineral assemblages are called "tHM suites" throughout the text and significant minerals are listed systematically in order of abundance (high to low). The complete heavy-mineral dataset including information on analyzed size classes is provided in Appendix Table A3.

5.3. Detrital geochronology

Detrital zircons were identified by Automated Phase Mapping (Vermeesch et al., 2017) with a Renishaw inVia^{TM} Raman microscope on the heavy-mineral separates of 42 samples, concentrated with standard magnetic techniques and directly mounted in epoxy resin without any operator selection *via* hand picking. The same size class used for heavy mineral analyses was thus considered for each sample. U-Pb zircon ages were determined at the London Geochronology Centre using an Agilent 7900 LA-ICP-MS (laser ablation-inductively coupled plasma-mass spectrometry) system, employing a NewWave NWR193 Excimer Laser operated at 10 Hz with a 25 μm spot size and ~2.5 J/cm^2 fluence. No cathodo-luminescence imaging was conducted. The laser spot was always placed blindly in the middle of zircon grains to treat all samples equally and avoid bias in intersample comparison ("blind-dating approach" illustrated and discussed in Garzanti et al., 2018b). No common Pb correction was applied. The mass spectrometer data were converted to isotopic ratios using GLITTER 4.4.2 software (Griffin et al., 2008) employing Plešovice zircon (Sláma et al., 2008) as a primary age standard and GJ-1 (Jackson et al., 2004) as a secondary age standard obtaining an average age of 605.05±1.37 (n=17; MSWD=5.2). A NIST SRM612 glass was used as a compositional standard for U and Th concentrations. GLITTER files were post-processed in R using IsoplotR 2.5 (Vermeesch, 2018). We used $^{206}Pb/^{238}U$ and $^{207}Pb/^{206}Pb$ as preferred ages for zircons younger and older than 1100 Ma, respectively. Additionally, we calculated concordia ages as the maximum likelihood intersection between the concordia line and the error ellipse of $^{207}Pb/^{235}U$ and $^{206}Pb/^{238}U$ ages (Ludwig, 1998). The discordia cutoff was set as +6.8 and -2.3 based on the Aitchison distance from the measured log ratio and the concordia line (Vermeesch, 2021). Overall, 5459 ages were obtained; the 3433 concordant ages (63%) were used for statistical analysis. The complete geochronological dataset is provided in Appendix B.

5.4. Graphical/statistical tools

The statistical tools applied to the analysed sand samples include Multidimensional Scaling (MDS; Kruskal and Wish, 1978; Vermeesch, 2013). This multivariate ordination technique takes a dissimilarity matrix as input and produces a map of samples as output, in which similar samples plot close together and dissimilar samples plot far apart. For detrital zircon U-Pb age spectra, a dissimilarity matrix can be constructed using the Kolmogorov-Smirnov statistic (i.e., the maximum vertical difference between two cumulative distribution functions; Feller, 1948).

To illustrate heavy-mineral data we used the compositional biplot (Gabriel, 1971), a statistical/graphical display that allows discrimination among multivariate observations (points) while shedding light on the mutual relationships among multiple variables (rays). The length of each ray is proportional to the variance of the corresponding variable in the dataset. If the angle between two rays is close to 0°, 90° or 180°, then the corresponding variables are correlated, uncorrelated, or inversely correlated, respectively.

6. Mineralogy of river sands

The main rivers that drain into the Kalahari Basin are sourced in the humid regions of Angola and Zambia in the north. The Caculuvar and Mucope tributaries of the Cunene River, draining the western edge of the Kalahari Erg in Angola (Fig. 1A), carry pure quartzose sand with a few K-feldspar grains. The extremely poor, zircon-rich tHM suite includes epidote, tourmaline, and minor andalusite, staurolite and rutile (Table 1). The Okavango and Cuando Rivers, which are also sourced in Angola and drain the northern Kalahari Basin towards the Caprivi Strip and Botswana, carry pure quartzose sand (Fig. 4I) with extremely poor, tourmaline-zircon-epidote-staurolite-kyanite-rutile tHM suites.

Sand carried by the upper Zambezi River in Zambia is also pure quartzose (Fig. 4K) with a poor tHM suite dominated by ZTR minerals with common kyanite, staurolite, and minor epidote. Clinopyroxene appears downstream of Ngonye Falls, increases towards Victoria Falls, and becomes rapidly predominant along the gorges downstream.

Zambezi tributaries in Zimbabwe include the Matetsi, which carries quartzo-lithic basalticlastic sand (Fig. 4M) with extremely rich tHM suites containing clinopyroxene exclusively, and the Gwai, which carries feldspatho-quartzose sand (Fig. 4O) with a poor tHM suite containing amphibole, subordinate epidote and garnet, and minor clinopyroxene, kyanite, and sillimanite. The Shangani, a Gwai tributary (Fig. 1A), carries quartzose sand with basaltic rock fragments, a few plagioclase grains, and a moderately rich tHM suite dominated by clinopyroxene.

In northern and central Namibia, the Omatako carries feldspatho-quartzose sand with K-feldspar >> plagioclase and a very poor tourmaline-amphibole-garnet tHM suite. The Okakongo (a northern tributary of the Swakop River draining towards the Atlantic Ocean) carries feldspar-rich feldspatho-quartzose sand (Fig. 4A) with moderately rich hornblende-dominated tHM suite. The Rietfontein carries pure quartzose sand (Fig. 4C) with a very poor staurolite-tourmaline tHM suite.

The White Nossob and Black Nossob (western and eastern branches of the Nossob River) carry feldspatho-quartzose sand containing granitoid and high-rank metamorphic rock fragments (Fig. 4E) with a moderately poor amphibole-garnet-staurolite-epidote tHM suite, and quartz-rich feldspatho-quartzose sand containing low-rank metasedimentary rock fragments with a moderately poor staurolite-epidote-garnet-zircon tHM suite, respectively.

The Molopo River, which drains the southern Kalahari, carries quartz-rich feldspatho-quartzose sand with common monocrystalline quartz displaying abraded overgrowths, plagioclase > K-feldspar, and a few shale/slate or quartzose sedimentary and metasedimentary rock fragments (Fig. 4G). The moderately poor tHM suite includes epidote, amphibole, ZTR minerals, garnet, clinopyroxene, and minor staurolite and kyanite.

7. Mineralogy of aeolian-dune sands

Dune sand is quartz-rich over most the vast Kalahari Basin: out of the 57 studied samples, 31 are pure quartzose, 12 quartzose, and 10 quartz-rich feldspatho-quartzose (Fig. 5). Throughout the northern Kalahari, in Angola, northeastern Namibia, Caprivi Strip, northern Botswana and western Zambia, sand consists virtually exclusively of monocrystalline quartz commonly showing rounded to subrounded outline and abraded overgrowths (Fig. 4L). Aeolian sand in the Caprivi Strip contains abundant red iron-oxide particles.

Pure quartzose sand also characterizes the eastern edge of the Kalahari in Zimbabwe as well as the central part of the sand sea from eastern Namibia to southeastern Botswana. In all these regions, K-feldspar prevails among the few feldspar grains, lithics are rare or lacking, and tHM assemblages are very poor to extremely poor and dominated by ZTR minerals. Staurolite is widespread, most common in the Ghanzi area (Fig. 4D) and generally associated with kyanite and minor andalusite. Kyanite increases progressively southwards in westernmost Zambia and is most abundant to the west of the Cuando/Zambezi confluence, where it is associated with minor garnet. Epidote is common south of the Okavango inland delta, where a few amphibole grains occur. Garnet is rare or lacking altogether (Table 1).

Basaltic detritus including rock fragments, plagioclase and clinopyroxene is significant in dune sand NW of Victoria Falls, and dominant in litho-quartzo-feldspathic dune sand close to the Zambezi gorges downstream (Fig. 4N).

In western Zimbabwe, dunes are markedly enriched in feldspars. In the NW near Masuma, aeolian sand is feldspatho-quartzose (Fig. 4P) with plagioclase > K-feldspar, quartz-rich siltstone/sandstone and medium-rank metamorphic rock fragments, biotite, and a moderately rich garnet-epidote tHM suite. In the SE near Bulawayo, aeolian sand is quartzo-feldspathic with K-feldspar > plagioclase and a poor amphibole-epidote suite. In eastern Botswana around the Makgadikgadi Pan, aeolian sand is quartzose, with K-feldspar > plagioclase and a very poor tHM suite with common epidote, ZTR minerals, amphibole and/or clinopyroxene, and minor kyanite, garnet and staurolite. Polycrystalline quartz, a few felsic volcanic, and quartz-rich siltstone/sandstone rock fragments are locally significant. Calcareous grains including common ooids occur in mounds on the surface of the Ntwetwe (western Makgadikgadi) Pan (Fig. 4J; McFarlane and Long, 2015).

Straddling the Botswana/South Africa border, aeolian dunes consist of quartzose to pure quartzose sand (Fig. 4H) with K-feldspar > plagioclase, and very poor tHM suites dominated by ZTR minerals with locally common epidote or staurolite. The Koppieskraalpan dune is quartz-rich feldspatho-quartzose with a few basaltic rock fragments, plagioclase > K-feldspar, and a moderately rich tHM suite including dominant clinopyroxene and subordinate garnet.

In the western Kalahari, SW of the Nossob River, aeolian-dune sand is relatively homogeneously quartzose to quartz-rich feldspatho-quartzose with K-feldspar >> plagioclase (Fig. 4F). The mostly poor and epidote-dominated tHM suite includes ZTR minerals and staurolite. Amphibole with minor clinopyroxene are significant in the northern Hardap region, staurolite with subordinate kyanite most common in SW Namibia, and garnet common in South Africa.

In northern Namibia, mineralogy is more varied. The Okahandja dune is feldspar-rich feldspatho-quartzose (Fig. 4B) with plagioclase > K-feldspar, up to high-rank metasedimentary rock fragments, common biotite, and a moderately rich tHM suite dominated by hornblende with clinopyroxene, ZTR minerals, apatite, and epidote. In the central region, aeolian sand is quartzose to pure quartzose, with K-feldspar >> plagioclase and poor tHM suites including mainly ZTR minerals, epidote, kyanite associated with either staurolite or garnet, and locally clinopyroxene. Quartzose sandstone and shale rock fragments may occur. In northwesternmost Botswana, the Qangwa dune is quartz-rich feldspatho-quartzose with plagioclase > K-feldspar and a moderately poor, epidote-dominated tHM suite including ZTR minerals.

8. Ages of detrital zircons

Five age ranges recur among the analysed samples (Fig. 6), corresponding to main orogenic episodes in southern Africa (Hanson, 2003; Dirks et al. 2009; Andersen et al., 2016, 2018): I) Limpopo (2.5-2.8 Ga, Neoarchean; peak at 2720 Ma); II) Eburnean (1.8-2.05 Ga, Orosirian; peak at 1893 Ma); III) Sinclair-Kibaran (1.2-1.4 Ga, Ectasian; peak at 1312 Ma); IV) Namaqua-Irumide (1.0-1.1 Ga, Stenian; peak at 1056 Ma); V) Damara-Lufilian (0.45-0.65 Ga, Ordovician-Cryogenian; peak at 581 Ma). Younger ages include a minor 'Karoo' cluster (220-320 Ma, Triassic-Pennsylvanian; peak at 266 Ma) and some Early Cretaceous ages (120-135 Ma) associated with magmatism related to South Atlantic rifting (e.g., Trumbull et al., 2004). Even younger grains (59-70 Ma, Paleocene-latest Cretaceous) associated with post-rift alkaline magmatism (Moore et al., 2008) sporadically occur in Botswana.

In provenance interpretation, it must be kept in mind that the ages of zircon grains in sediments reflect their crystallization age, which may not — and in general does not — necessarily correspond to the age of the source rock, because zircon is a durable mineral that can be recycled even multiple times. The U-Pb age spectra of detrital zircons, therefore, only allow us to discriminate among the different ages of the original crystalline source rocks (i.e., protosources *sensu* Andersen et al., 2016), whereas the proportion of first cycle *versus* even multiply recycled zircon grains can be evaluated only qualitatively for each sample based on petrographic composition and heavy-mineral concentration (Garzanti, 2016).

Data obtained in this study are compared with previously obtained radiometric ages on diverse crustal domains across southern Africa compiled from numerous literature sources (Fig. 7). The age compilation is summarized in Table 2 and presented in full in Appendix C. Further extensive information on bedrock ages in the region are contained in Gärtner et al. (2014) and Goscombe et al. (2020).

8.1. River sands

The zircon-age spectrum in sand of the Mucope River, draining entirely within the northwestern Kalahari dunefield in Angola, displays a unimodal Orosirian peak at ~1.96 Ga, identifying the Eburnean Angola Block as the main protosource (Fig. 6).

Detrital-zircon U-Pb age patterns in Okavango and Cuando sands are similarly characterized by Ediacaran-Cryogenian and Stenian peaks, with a major Orosirian cluster and a minor Neoarchean cluster. Upper Zambezi sand is similar but with notably less Neoarchean ages, and both Orosirian and Neoarchean ages become rarer in its Zambian tributaries (Fig. 6). These rather homogeneous zircon-age signatures across the northern part of the Kalahari Basin reflect extensive recycling of sediment originally derived from mainly Eburnean, Irumide, and Damara protosources. In contrast, Gwai River sand in Zimbabwe yielded a polymodal zircon-age spectrum indicating major Neoarchean and Eburnean, and minor Irumide and Pan-African protosources.

8.2. Aeolian-dune sands

Pure quartzose dune sands in the Okavango region, from the inland delta to the Makgadikgadi Pan, yielded multimodal zircon-age spectra characterized by Ediacaran, Stenian, and Orosirian peaks. Similar spectra, with more Cryogenian to Stenian ages and less Paleoproterozoic to Neoarchean ages, are displayed by pure quartzose aeolian-dune sand along the upper Zambezi valley, reflecting more Damaran and Irumide, and somewhat less Eburnean protosources (Fig. 7).

In Zimbabwe, pure quartzose aeolian sand at the eastern edge of the Kalahari Basin is characterized by similar age spectra with major Ediacaran and Stenian peaks, subordinate Orosirian, and minor Neoproterozoic clusters. In western Zimbabwe, instead, the feldspatho-quartzose Masuma dune yielded a few Stenian, Orosirian-Rhyacian, and Archean zircon ages, whereas Archean-aged zircons occur in quartzo-feldspathic dune sand near Bulawayo (Fig. 6).

In Botswana south of Makgadikgadi Pan, Paleozoic ages increase slightly, and Orosirian ages decrease. Farther south, the quartzose Mokgomane dune near Gaborone is singled out by the common Neoarchean to Mesoarchean zircons pointing at cratonic protosources (Fig. 7A, 7B), whereas Stenian and subordinate Cryogenian zircons increase progressively westwards in pure quartzose to quartz-rich feldspatho-quartzose dune sand along the Molopo River course in the southern Kalakari (Fig. 6).

In Namibia, Ordovician to Ediacaran ages predominate in feldspar-rich feldspatho-quartzose to quartzose dune sand, reflecting prominent Damara protosources (Fig. 6). Along a SW/NE traverse in northern Namibia, pure quartzose aeolian sand yielded multimodal, Permo-Triassic, Cambrian to Ediacaran, Stenian, Orosirian and minor Neoarchean clusters. The quartz-rich feldspatho-quartzose Qangwa dune located near the Aha Hills in NW Botswana is singled out by its nearly unimodal spectrum with early Tonian age peak at 956 Ma (Fig. 6).

Along a W/E traverse between Windhoek in central Namibia and the Ghanzi Ridge in Botswana, pure quartzose aeolian sand yielded mainly Orosirian, Statherian, and Stenian zircon ages in the west, mainly Stenian to Ectasian ages in the center, and mainly Cambrian to Ediacaran ages in the east (Okahandja dune).

Quartzose to quartz-rich feldspatho-quartzose aeolian sand in the western Kalahari (WK in Fig. 6) yielded mostly Mesoproterozoic (Ectasian and subordinately Stenian) zircon ages and no ages younger than 500 Ma, indicating mainly Sinclair and Namaqua protosources.

9. Provenance of Kalahari aeolian-dune sand

In most of the Kalahari Basin, including the NWK and NEK dunefields in Angola, Namibia and Zambia, much of Botswana, and part of the EK dunefield in Zimbabwe, dune sand is dominated by monocrystalline quartz associated with very poor tHM suites including durable ZTR minerals, staurolite, and kyanite (Figs. 8, 9, and 10). Such a homogenized mineralogical signature reveals multiple recycling of older quartzose sandstones through geological time.

A local exception is the quartz-rich feldspatho-quartzose sand of the Qangwa dune collected near the Aha Hills, which contains a moderately poor, epidote-dominated tHM suite with zircon grains yielding mostly Tonian-Stenian ages (peak between 900 and 950 Ma; Fig. 6). This suggests recycling of Neoproterozoic siliciclastic rocks exposed nearby (e.g., Ghanzi Group; Baillieul, 1975; Hall et al., 2018), whereas the few Statherian-Orosirian ages point at minor protosources in the Angola Block to the north (McCourt et al., 2013).

At the other extreme, aeolian dunes situated at the opposite margins of the Kalahari, near exposures of crystalline basement in central Namibia or of Karoo basalts in Zimbabwe, reveal mainly first-cycle provenance and limited mixing with recycled aeolian sand of the erg (Fig. 10). Litho-quartzo-feldspathic composition with dominant plagioclase, clinopyroxene, and mafic volcanic rock fragments derived from Karoo lavas characterizes aeolian-dune sand near the basaltic gorges carved by the Zambezi River downstream of Victoria Falls, where less than a fourth of the bulk sediment is represented by aeolian monocrystalline quartz (i.e., less than in local right-bank Zambezi tributaries draining into the Karoo volcanic rocks; cf. Figs. 4M and 4N).

The aeolian dune located on the Zimbabwe Craton near Bulawayo (Fig. 3) is singled out by its quartzo-feldspathic composition with high-rank metamorphic rock fragments, amphibole-epidote tHM suite, and Archean-aged zircon grains, reflecting provenance from local cratonic basement. The feldspatho-quartzose Masuma dune yielded a moderately rich garnet-dominated tHM suite with subordinate epidote and most zircon grains dated between 2.0 and 3.4 Ga (Fig. 6), indicating largely local provenance from the metamorphic basement of the Dete/Kamativi Inlier belonging to the Paleoproterozoic Magondi Belt (Fig. 7B; Glynn et al., 2020).

On the western side of the Kalahari, the Okahandja dune has feldspar-rich feldspatho-quartzose composition with moderately rich amphibole-dominated tHM suite (Figs. 8 and 9) and mainly Cambrian-Ediacaran zircon grains, indicating provenance dominantly from amphibolite-facies metamorphic rocks exposed in the inland branch of the Damara orogen (Jung et al., 2007).

Consistently quartz-rich feldspatho-quartzose to quartzose composition and poor tHM suite including common epidote associated with ZTR minerals and staurolite characterize sand in the western Kalahari dunefield, where detrital-zircon ages are mostly Mesoproterozoic (Ectasian to

Stenian with peak around 1.3 Ga, and subordinately late Paleoproterozoic with peak around 1.8 Ga). Aeolian sand is inferred to have been fed from Damara, Nama, and Karoo sedimentary and metasedimentary rocks, together with arc-related low-grade metasedimentary and magmatic rocks of the Rehoboth terrane in the northwest (Fig. 3; Becker et al., 2006). Clinopyroxene occurs in the northern Hardap region, reflecting minor contribution from locally exposed Karoo basalts (Fig. 3). Petrographic composition is similar in the adjacent western southern Kalahari (wSK) dunefield, where garnet notably increases (Fig. 10) and detrital-zircon ages are mainly Stenian (peak around 1.07 Ga), indicating extensive recycling of the Nama Group (Blanco et al., 2011; Andersen et al., 2018). The moderately rich, clinopyroxene tHM suite of the Koppieskraalpan dune in the wSK dunefield (Fig. 2A) reveals minor local supply from Karoo lavas.

Transitional quartzose sand containing mostly K-feldspar with locally dominant microcline* and mostly very poor tHM suites — including ZTR minerals as well as epidote, kyanite, staurolite, and locally common clinopyroxene or some amphibole — characterizes aeolian dunes in parts of Zambia (upper Zambezi valley), Botswana (e.g., Makgadikgadi and Gaborone areas), northern South Africa, and central-northern Namibia (Fig. 10). Clinopyroxene dominates the tHM suite of the aeolian dune in the Zambezi valley shortly upstream of Victoria Falls, testifying to minor local first-cycle supply from Karoo basalts. Garnet is relatively common in central-northern Namibia, where half of zircon grains yielded Ordovician-Ediacaran ages indicating contribution from the northern Damara Belt nearby (Fig. 7B; Lehmann et al., 2016).

10. Fluvial-aeolian interactions and multistep recycling

The mineralogical composition of aeolian dunes and its variability across a sand sea reflect the relative importance of fluvial and aeolian processes and the degree of their interplay. Sand seas largely fed by river systems are typically characterized by partly first-cycle detritus including various amounts of diverse types of rock fragments, feldspars and heavy minerals, generally allowing identification of a single dominant source, as for the Namib Erg (Garzanti et al., 2012).

The opposite end member is represented by dunefields where sand is dominantly generated *in situ* from disaggregation of locally exposed rocks with high sand-generation potential (e.g., quartz-rich sandstones) and next reworked and homogenized by winds during several sedimentary cycles. In these cases, sand typically bears a distilled homogenous composition consisting almost exclusively of mostly rounded monocrystalline quartz associated with an extremely poor tHM suite dominated by durable ZTR minerals, as for the Sahara Desert (Pastore et al., 2021).

The geographic distribution of such contrasting desert types is mainly controlled by precipitation in adjacent highlands fuelling fluvial discharge. In hyper-arid tropical deserts dominated by aeolian dynamics, such as the Sahara or the Great Nafud in Arabia, river action may be weakened to the point that fluvial supply to the aeolian system becomes insignificant. Conversely, dry river valleys are invaded by pure quartzose windblown sand, thus erasing all local sources of mineralogical heterogeneity (Garzanti et al., 2013, 2015a p.46). Fluvial sources are instead readily identified for dunefields accumulated in drylands at the foot of high mountain areas, as in central Asia or Argentina (e.g., Rittner et al., 2016; Garzanti et al., 2019a, 2020, 2021b).

The Kalahari Basin — which extends over twenty degrees of latitude, is characterized by a pronounced increase in precipitation from the southwest to the subequatorial north, and has seen repeated changes in climatic conditions through the recent and less recent past — provides both end-member examples, as well as a series of intermediate situations. Sand mineralogy is rather homogeneously pure quartzose in the north (NWK, NEK, and EK dunefields), closer to humid equatorial regions, but presents peculiar feldspar-rich or even lithic-rich compositions at both western and eastern margins of the erg, where detrital modes with more abudant and varied tHM suites indicate largely first-cycle supply from local rivers (Fig. 10).

Intermediate is the case of the WK dunefield in SE Namibia, where sand is quartz-rich but with a significant amount of mostly K-feldspar, a few lithic fragments, and an up to moderately poor tHM suite including not only epidote and staurolite but locally also amphibole and pyroxene, reflecting the contribution of fluvial sediments (cf. Figs. 4E and 4F).

In the NWK and NEK dunefields, as in Botswana, the coexistence of pure quartzose sand both in rivers (Mucope, Okavango, Cuando, upper Zambezi, Rietfontein) and adjacent aeolian dunes (cf. Figs. 4C and 4K with 4D and 4L) makes it hard to discern how much of the river sand has ended up in the dunes and, *vice versa*, how much of the river sand has been supplied by erosion and reworking of the dunes. Overall, most of the sand in all the above-mentioned rivers must have been ultimately derived from reworking of Kalahari Group sediments, as most reliably assessed for Angolan rivers that drain entirely within the erg (e.g., Mucope and Cuando). It is noteworthy that both fluvial and aeolian sands along the final Chobe tract of the Cuando River get notably enriched in kyanite. This reveals mixing with sand originally fed by the upper Zambezi and reworked by the Cuando from the toe of the alluvial fan previously built by the Zambezi across the Okavango rift, between Lake Liambezi in the west and the Chobe depression in the east (Lake Caprivi of Shaw and Thomas, 1988).

In the opposite case, feldspar-rich or lithic-rich aeolian-dune sand with similar mineralogy as river sediments nearby points to partly first-cycle origin and chiefly fluvial supply, followed by wind deflation and accumulation at the margins of the Kalahari with limited mixing with aeolian quartz of the erg (cf. Figs. 4A, 4M, and 4O with 4B, 4N, and 4P). The proportion of aeolian Kalahari sand reworked in river sediments is readily identified by commonly rounded to subrounded monocrystalline quartz and thus easily calculated in this case. Overwhelming in the Caculuvar, Mucope, Okavango, Cuando, and Rietfontein Rivers (Figs. 4C and 4I), reworked aeolian quartz represents more than 90% of bulk sand in the upper Zambezi (Fig. 4K) and still ~85% upstream of Lake Kariba despite progressively increasing volcaniclastic supply across the basaltic gorges downstream of Victoria Falls. In Zambezi tributaries of western Zimbabwe, aeolian quartz is estimated to range from a minimum of ~35% in Matetsi sand up to 80-85% in Upper Gwai and Shangani sands (Garzanti et al., 2014a). Recycled aeolian monocrystalline quartz with rounded outlines or abraded overgrowths accounts for a large majority of Molopo River sand (Fig. 4G).

11. Paleoweathering in the Kalahari

The extent to which a sediment has been subjected to chemical weathering, integrated over a series of sedimentary cycles, can be evaluated by combining evidence from petrographic, heavy-mineral, clay-mineral, and geochemical data.

Distilled multicyclic sand of northern Kalahari aeolian dunes and of the Okavango, Cuando, and upper Zambezi Rivers is composed dominantly of quartz with strongly depleted tHM suites including zircon, tourmaline, rutile, staurolite, and kyanite but virtually no garnet or apatite (both invariably ≤ 1%tHM; Table 1). The scarcity of garnet relative to staurolite, kyanite, andalusite, and sillimanite [G/(G+SKA) < 5% in both aeolian and fluvial sands; Fig. 10] is anomalous, because these minerals are associated in amphibolite-facies metapelites and unweathered detritus derived from them, where garnet is typically dominant [G/(G+SKA) = 70±20%; Garzanti et al., 2006, 2010].

The Okavango and Zambezi Rivers carry mud containing ~40% kaolinite (i.e., more than most other rivers in tropical southern Africa; Garzanti et al., 2014b). Northern Kalahari aeolian dunes are strongly depleted in virtually all chemical elements but Si. Even Zr and Hf are low in both aeolian and fluvial sands (83±55 and 2±1 ppm *versus* 190 and ~6 ppm in the Upper Continental Crust standard; Taylor and McLennan, 1995), suggesting that all minerals including zircon are depleted relative to most durable quartz. Among chemical indices of weathering, $\alpha^{Al}{}_{Na}$ is > 3 in Okavango, Cuando, and upper Zambezi fluvial sands, reaches > 5 in aeolian-dune sand, and is ~20 in mud Garzanti et al., 2014a, 2014b). The traditional WIP and CIA indices (Parker, 1970; Nesbitt and Young, 1982) reach down to 0 and up to ≥ 80 in aeolian sand (down to 1 and up to ≥ 90 in fluvial sand), with consequently extreme CIA/WIP ratio reflecting extensive recycling (Garzanti et al., 2019b).

Pure quartzose sand lacking garnet in presence of common staurolite and kyanite, abundance of kaolinite in mud, and chemical indices pointing at high weathering intensity cannot be the product of a single sedimentary cycle in the current climatic setting. They require widespread recycling of sediments affected by extensive weathering in chemically much more aggressive hot-humid climates of the past. All these pieces of evidence combined cannot be explained with breakdown of all but the most durable minerals by grain-to-grain aeolian impacts, which prove to be effective enough to round sand-sized silicate grains but far from efficient enough to systematically destroy them mechanically (Garzanti et al., 2015b; Rittner et al., 2016; Resentini et al., 2018). Detrital components of northern Kalahari aeolian sand must have undergone very extensive weathering in humid subequatorial climate before being recycled during repeated episodes of alternating fluvial and wind erosion, leading to their accumulation in the erg. In other words, they represent the echo of paleo-weathering stages passed on to the present landscape through multiple recycling episodes.

12. Drainage integration as a driver of provenance change

Sand seas such as the Kalahari or the Great Nafud and Rub'Al Khali in Arabia are huge reservoirs of quartz-rich polycyclic sand trapped in the continental interiors. In the hyperarid climate of the tropics, precipitation and runoff can be so scarce that ephemeral rivers are unable to carry sediment across and beyond these vast rift-related sags, where sand is dumped and multiply reworked while remaining largely untapped for tens or even hundreds of million years. An analogous ancient case is the late Mesozoic Botucatu paleoerg, drained today by the Paraná-Uruguay river system in South America (Bertolini et al., 2020).

In Arabia, sand seas are dominated by aeolian processes that drag sand uphill for hundreds of kilometers from the Gulf coast inland across the Rub' Al Khali (Garzanti et al., 2003, 2017). Only a trivial amount of aeolian sand has started to escape towards the Indian Ocean *via* Wadi Hadhramaut-Masila, since this rather large but ephemeral river broke through the carbonate tableland representing the northern shoulder of the Gulf of Aden rift (Garzanti et al., 2001). In the case of the Sahara, the Nile is the only river that, before closure of the Aswan High Dam in 1964, possessed sufficient discharge and competence to carry as far as the sea Saharan sand and silt (estimated as ~10% of total sediment load, which used to vary between ≤ 50 and ≥ 300 million tons/year; Inman and Jenkyns, 1984; Garzanti et al., 2015a). This is between one and two orders of magnitude less than the volume of dust blown off the Sahara towards and beyond the Atlantic Ocean and the Mediterranean Sea, estimated to range between 130-460 and 1400 million tons/year overall (Goudie and Middleton, 2006; Stuut et al., 2009 and references therein).

The amount of dust emissions from the Kalahari is much lower than for the Sahara (Crouvi et al., 2010; Bhattachan et al., 2013) and sediment exported to the ocean notably less even though diverse major rivers draining the dryland reach the coast. To the west, Kalahari sand supply to the Atlantic Ocean cannot be estimated with forward-mixing calculations for the Congo River because it carries sediment overwhelmingly recycled from multiple quartzose sandstone units, it may represent up to 30% of Cuanza River sand (annual sediment load 0.6±0.1 million tons, 43% mostly fine sand; Holisticos, 2012), but it is very minor for the Cunene River (although recycled aeolian sand accounts for ~15% of Cunene sand at the western edge of the Kalahari) and negligible for the Orange River (based on petrographic and heavy-mineral data in Garzanti et al., 2014a, 2018a). To the east, Kalahari sand is conveyed towards the Indian Ocean almost exclusively by the Zambezi River (annual sediment flux between 20 and 100 million tons; Hay, 1998). Kalahari aeolian quartz grains representing ~85% of upper Zambezi sand are all trapped in Lake Kariba at present, but Kalahari sand accounted for no more than 10% of total Zambezi bedload even before dam construction (Garzanti et al., 2021a). The total volume of Kalahari sand exported towards the oceans is thus of the same order of magnitude as the endorheic Okavango sediment flux (between 0.2 and 2 million tons of mostly bedload sand recycled from Kalahari aeolian dunes; Shaw and Thomas 1992). Hence, less than half of the sand eroded from Kalahari dunes is exported towards the ocean today.

This budget, however, may have changed drastically and repeatedly in the past, and may change again in the future depending on climatic conditions as well as on the balance between rejuvenated subsidence in the Okavango Graben *versus* rejuvenated uplift of the African superswell (Kinabo et al., 2007; Al-Hajri et al., 2009). River piracy plays a fundamental role too, as emblematically documented on both flanks of the Kalahari Plateau by the recent capture of formerly endorheic Cunene and Zambezi drainage by headward eroding coastal rivers. Capture of the upper Zambezi by the middle Zambezi is generally held to have occurred around early Pleistocene time (Moore et al., 2007) but the upper Zambezi returned to be at least partly endorheic in the mid-Pleistocene, as inferred from diverse mega-lake Makgadikgadi phases through the late Pleistocene (Burrough et al., 2009b; Moore et al., 2012). During this period of partly endorheic Zambezi floods (Burrough et al., 2008), repeated drainage changes were induced by the evolution of the Okavango Graben (Vainer et al., 2021b). This tectonic depression finally diverted the Cuando River towards the Zambezi and is presently favoring the capture of the Okavango as well, conveyed eastward along the Selinda spillway (Fig. 2; Gumbricht et al. 2001).

In a deeper past, a marked increase in monocrystalline quartz grains with rounded to subrounded outline and abraded overgrowths is documented in post-Tortonian strata of the Zambezi Delta subsurface (Chanvry et al., 2018), pointing to a sudden flux of recycled quartz-rich Kalahari sand from the continental interiors. A similar episode may well be repeated in the future if the capture of the entire Okavango by the Zambezi River will proceed to the point that most of recycled Kalahari sand is conveyed towards the Indian Ocean.

This argument highlights how tapping of huge sand reservoirs in continental interiors represents — besides tectonic activity, climate-induced weathering, or dissolution during diagenesis — an effective potential factor that can produce significant pulses of mineralogical change (e.g., stepwise up-section increase of recycled quartz grains) in coastal passive-margin and continental-embankment successions.

13. Conclusions

Aeolian dunes of the Kalahari are homogeneously pure quartzose in Angola, Zambia, and over much of Botswana and parts of Zimbabwe and Namibia, where they also contain a few K-feldspar grains and strongly depleted heavy-mineral assemblages dominated by ZTR minerals and including common staurolite in Botswana and kyanite in Zambia, but virtually no garnet. Composition varies markedly only at the western and eastern edges of the erg, ranging from feldspar-rich feldspatho-quartzose and hornblende-rich in the Damara Belt of central Namibia to quartzo-feldspathic and hornblende-rich in the Zimbabwe Craton or litho-quartzo-feldspathic and clinopyroxene-rich beside the Zambezi basaltic gorges near Victoria Falls. Compositionally distinct is the partially active western Kalahari dunefield of SE Namibia, where sand is quartzose to quartz-rich feldspatho-quartzose with common epidote, indicating partly first-cycle but largely polycyclic provenance from Mesoproterozoic crustal domains, Damara Belt, and Nama and Karoo Groups.

U-Pb age spectra of detrital zircons allow discrimination among protosources of different ages in various parts of the erg. Damara ages (0.45-0.65 Ga) are widespread and most abundant in aeolian dunes of central Namibia but quite rare in the western Kalahari dunefield to the south. Namaqua-Irumide Stenian ages (1.0-1.1 Ga), also widespread, are particularly common in aeolian dunes along the Botswana/South Africa border, increasing southward towards the Namaqua Belt. Sinclair Ectasian ages (1.2-1.4 Ga) are most abundant in the western Kalahari dunefield of SE Namibia. Eburnean Orosirian ages (1.8-2.05 Ga) are most frequent in Angola and northernmost Botswana. Neoarchean ages characterize aeolian dunes at the edge of the Zimbabwe and Kaapvaal Cratons in SW Zimbabwe and SE Botswana.

The compositional fingerprints of aeolian-dune sand and their variability reflect the degree of interaction between fluvial and aeolian processes across the sand sea. In northern Kalahari dunefields adjacent to humid subequatorial regions, widespread monocrystalline quartz commonly showing abraded overgrowths combined with strongly depleted ZTR-rich heavy-mineral assemblages lacking garnet but containing staurolite and kyanite, common kaolinite in river muds, and geochemical indices reveal that the sediments have undergone very extensive weathering in humid subequatorial climate before being stored into the erg. The composition of aeolian-dune sand thus reverberates the echo of paleo-weathering passed on to the present landscape through multiple recycling episodes.

Intracratonic sag basins such as the Kalahari, straddling the arid tropical belt, contain vast amounts of quartz-rich polycyclic sand. Whenever tectonic or climatic conditions favor the development of an integrated drainage system connecting the continental interiors with the coast, tapping into such a huge sediment reservoir may induce a sudden pulse of quartz-rich sand to the oceans and thus a significant mineralogical change in continental-embankment successions. Such an event, recorded in post-Tortonian sediments of the Zambezi Delta, may occur again in the future if development of the Okavango rift will lead to the incorporation of the entire Okavango River to the Zambezi drainage system.

Acknowledgments

Several samples from Kalahari aeolian dunes were obtained thanks to the generosity of Sallie Burrough, Tom Kemp, and Matt Telfer; some fluvial samples were provided by Hella Wittmann, Hanna Haedke, Armanda Trindade, Dario Fornara, Lindani Ncube, and Helena Johanna Van Niekerk. Most petrographic and heavy-mineral analyses were made by Giuditta Radeff, Marta Padoan, and Mara Limonta. Marta Padoan helped substantially with the compilation of geochronological ages and Martin Rittner with geochronological analyses. Editor Chris Fielding and reviewers David Chew, Majie Fan, and Anonymous provided very useful constructive critical advice. This study was supported by MIUR – Dipartimenti di Eccellenza 2018–2022, Department of Earth and Environmental Sciences, University of Milano-Bicocca.

Appendices – Supplementary Data

Supplementary data associated with this article include information on sampling sites (Table A1), together with the complete bulk-sand petrography (Table A2), heavy mineral (Table A3), and detrital-zircon geochronology datasets (Appendix B). Appendix C presents a compilation of numerous radiometric ages from diverse literature sources on modern sands, ancient sandstones, and crustal domains in the areas described in this article. The Google-Earth™ map of sampling sites *Kalahari.kmz* is also provided.

FIGURE AND TABLE CAPTIONS

Figure 1. The vast Kalahari Basin in southern Africa. A) Main regions and river courses. B) Relief map with sampling sites.

Figure 2. The Kalahari sand sea. **A**) Types of aeolian dunes, wind directions, and sand flow patterns (compiled after Thomas and Shaw, 1991, Nicholson, 1996, and Haddon, 2005). NWK, NEK, EK, WK, SK, and wSK = northwestern, northeastern, eastern, western, southern, and western southern Kalahari dunefields; **B**) Rainfall map, showing increase in precipitation from south to north and from west to east across southern Africa. **C**) Distribution of climatic zones (Köppen–Geiger classification; Kottek et al., 2006): A = equatorial; B = arid; C = warm temperate. Precipitation: W = desert; S = steppe; f = fully humid; s = summer dry; w = winter dry. Temperature: h = hot arid; k = cold arid; a = hot summer; and b = warm summer.

Figure 3. Geology of southern Africa (compiled after Schlüter, 2008 and other sources cited in text).

Figure 4. Comparison between the petrographic composition of fluvial and nearby aeolian-dune sands in the Kalahari Basin (photos arranged in geographical order: **A** to **H** from NW to SE in the west; **I** to **P** from W to E in the east). **A**, **B**: feldspar-rich feldspatho-quartzose sands (S4364 and E4875). **C**, **D**: pure quartzose sands (S4309 and E4889). Feldspatho-quartzose (**E**: S4313) and quartz-rich feldspatho-quartzose sands (**F**: NAM6/4/2). Quartz-rich feldspatho-quartzose (**G**: S5145) and pure quartzose sands (**H**: E5540). Pure quartzose sands (**I**: S4299, note weathered quartz to the right; **J**: NKALB, note ooids). **K**, **L**: pure quartzose sands (S4297 and E5481). Quartzo-lithic volcaniclastic (**M**: S4287) and litho-quartzo-feldspathic volcaniclastic sands (**N**: E4881, note rounded clinopyroxene). **O**, **P**: feldspatho-quartzose sands (S4284 and E4882). All photos with crossed polars; blue bar for scale = 100 µm.

Figure 5. Petrography and heavy minerals in river (circles; upper panel) and aeolian-dune sands (squares; lower panel). Q = quartz; F = feldspars; L= lithic fragments; ZTR = zircon + tourmaline + rutile; SKA = staurolite + kyanite + andalusite + sillimanite; AGE = amphibole + garnet + epidote. Besides sand largely derived from Karoo basalts in western Zimbabwe, samples plot along the Q/F leg of the triangle, with compositions ranging from quartzo-feldspathic (QF) and feldspatho-quartzose (FQ), to quartzose (Q) and pure quartzose (pQ) (compositional fields after Garzanti, 2019). The Q/F and ZTR parameters are indicators of selective chemical breakdown of less durable feldspars (generally plagioclase) and heavy minerals (largely garnet, amphibole, pyroxene, and epidote) integrated through repeated sedimentary cycles. Symbols for upstream samples in the same river system are smaller.

Figure 6. U-Pb age spectra of detrital zircons (age vs. frequencies plotted as Kernel Density Estimates using the *provenance* package of Vermeesch et al., 2016; blue panels = river sands; yellow panels = aeolian sands). Age fingerprints are homogenized in the northern and central Kalahari but distinct at the edges of the erg, where prominent Damara peaks in central Namibia and Archean ages in SW Zimbabwe to SE Botswana reflect the time structure of source rocks in southern Africa (Hanson, 2003; Gärtner et al., 2014). The complete dataset is presented in Appendix B.

Figure 7. Multidimensional scaling maps based on U-Pb age spectra of detrital zircons highlight the degree of sand homogenization across various parts of the Kalahari Basin (axes units are normalised values based on Kolmogorov-Smirnov distance). **A**) Comparison among age spectra of aeolian-dune (squares) and river (circles) sands presented in Fig. 6. Distinct provenance signatures are documented locally (69% of ages ≥ 2 Ga in western Zimbabwe dunes; 54% Orosirian-Rhyacian ages in Mucope sand; 55% Tonian ages in Qangwa dune; 67% of Cambrian-Ediacaran ages in Okahandja dune; 61% of Stenian-Ectasian ages in western and western southern Kalahari). **B**) Comparison among age spectra of aeolian-dune and major river sands from this study and literature data (stars) compiled in Table 2. **C**) Comparison between the cumulative age spectrum of aeolian-

dune and major river sands analysed in this study and all potential sources and protosources (stars; data compiled in Table 2). Closest and second closest neighbours are linked by solid and dashed lines, respectively. The goodness of fit is evaluated using the "stress" value of the configuration (0.2 = poor; 0.1 = fair; 0.05 = good; table 1 in Vermeesch, 2013).

Figure 8. Mineralogy of Kalahari aeolian-dune sands. The compositional biplot (drawn with CoDaPack software by Comas-Cufí and Thió-Henestrosa, 2011) discriminates among three sample groups: i) feldspar-rich dunes containing garnet, amphibole and epidote partly derived from basement rocks in western Zimbabwe and central Namibia; ii) clinopyroxene-rich volcaniclastic sand derived from Karoo basalts near Victoria Falls; iii) pure quartzose sand strongly depleted in all detrital components besides durable ZTR minerals, staurolite, kyanite and andalusite, dominating through the northern Kalahari and across the central erg in Botswana. Detritus from Precambrian rocks, significant in SE Namibia, is locally dominant at opposite edges of the erg in central Namibia and western Zimbabwe. Detritus from Karoo basalts, abundant near Victoria Falls, is only locally significant elsewhere. Lvm = volcanic and metavolcanic lithics; Lsm = sedimentary and metasedimentary lithics; tHMC =transparent heavy-mineral concentration; ZTR = zircron + tourmaline + rutile.

Figure 9. Comparison between the mineralogy of aeolian-dune (squares) and river (circles) sands. The correspondence between mineralogical signatures of fluvial and nearby aeolian dunes in western Zimbabwe and central Namibia indicates that pure quartzose polycyclic Kalahari sand mixes locally with first-cycle detritus from Archean to Cambrian bedrocks. Because of arid conditions and high-frequency climatic fluctuations, exchanges of sediment from river channels to dunefields and back have taken place repeatedly across the erg throughout the Quaternary. Parameters as in Figs. 5 and 8.

Figure 10. Provenance maps of the Kalahari Basin (aeolian dunes = squares; river sands = circles). Across most of the erg, aeolian dunes have homogenized pure quartzose composition with depleted

tHM suites lacking garnet. Mixing with locally supplied detritus including significant amounts of feldspars, rock fragments and heavy minerals including garnet occurs in seven areas: 1) inland branch of the Damara Belt; 2) SE Namibia; 3) near Aha Hills; 4) near Karoo basalts; 5) near Magondi Belt; 6) near Zimbabwe Craton; 7) near Kaapvaal Craton. Lack of garnet from north to south across the central erg indicates intense weathering inherited from previous climatic stages. G = garnet; SKA = staurolite + kyanite + andalusite + sillimanite; tHMC = transparent-heavy-mineral concentration.

Table 1. Petrography and heavy minerals in fluvial and aeolian-dune sands of the Kalahari. Q = quartz; F = feldspars (P = plagioclase); L = lithic grains (Lvm = volcanic to very low-rank metavolcanic; Lsm = sedimentary and metasedimentary); MI* = Metamorphic Index (Garzanti and Vezzoli, 2003). tHMC = transparent heavy minerals; ZTR = zircon + tourmaline + rutile; Ap = apatite; Ep = epidote; Grt = garnet; St = staurolite; Ky = kyanite; Amp = amphibole; Px = pyroxene; &tHM = other transparent heavy minerals (mostly andalusite, titanite, anatase, sillimanite, and locally olivine or monazite); n° = numer of samples.

Table 2. Age spectra of modern sands, ancient sandstones, and crustal domains in southern Africa (full dataset including 4224 ages from 107 literature sources provided in Appendix C). Age peaks and relative frequencies calculated with Density Plotter (Vermeesch, 2012).

REFERENCES

Al-Hajri, Y., White, N., Fishwick, S., 2009. Scales of transient convective support beneath Africa. Geology, 37(10), 883-886.

Allen, P.A., 2017. Sediment Routing Systems. The Fate of Sediments from Source to Sink. Cambridge University Press, Cambridge, 407 p.

Andersen, T., Kristoffersen, M., Elburg, M.A., 2016. How far can we trust provenance and crustal evolution information from detrital zircons? A South African case study. Gondwana Research, 34, 129–148.

Andersen, T., Elburg, M.A., van Niekerk, H.S., Ueckermann, H., 2018. Successive sedimentary recycling regimes in southwestern Gondwana: Evidence from detrital zircons in Neoproterozoic to Cambrian sedimentary rocks in southern Africa. Earth-Science Reviews, 181, 43-60.

Andò, S., Morton, A., Garzanti, E., 2014. Metamorphic grade of source rocks revealed by chemical fingerprints of detrital amphibole and garnet. In: Scott, R.A., Smyth. H.R., Morton, A.C., Richardson, N. (Eds.), Sediment provenance studies in hydrocarbon exploration and production. Geological Society London, Special Publication 386, 351-371.

Baillieul, T.A., 1975. A reconnaissance survey of the cover sands in the Republic of Botswana. Journal of Sedimentary Petrology, 45, 494-503.

Bateman, M.D., Thomas, D.S.G., Singhvi, A.K., 2003. Extending the aridity record of the Southwest Kalahari: current problems and future perspectives. Quaternary International, 111, 37-49.

Becker, T., Schreiber, U., Kampunzu, A.B., Armstrong, R., 2006. Mesoproterozoic rocks of Namibia and their plate tectonic setting. Journal of African Earth Sciences, 46, 112-140.

Bertolini, G., Marques, J.C., Hartley, A.J., Da‐ Rosa, A.A., Scherer, C.M., Basei, M.A., Frantz, J.C., 2020. Controls on Early Cretaceous desert sediment provenance in south‐ west Gondwana, Botucatu Formation (Brazil and Uruguay). Sedimentology, 67(5), 2672-2690.

Bhattachan, A., D'Odorico, P., Okin, G.S., Dintwe, K., 2013. Potential dust emissions from the southern Kalahari's dunelands. Journal of Geophysical Research: Earth Surface, 118(1), 307-314.

Blanco, G., Germs, G.J.B, Rajesh, H.M, Chemale, F., Dussin, I.A., Justino, D., 2011. Provenance and paleogeography of the Nama Group (Ediacaran to early Palaeozoic, Namibia): petrography, geochemistry and U–Pb detrital zircon geochronology. Precambrian Research, 187, 15-32.

Blenkinsop, T., Moore, A., 2013. Tectonic geomorphology of passive margins and continental hinterlands. In: Shroder, J.F. (Ed.), Treatise on Geomorphology. Academic Press, San Diego, vol. 5, pp. 71-92.

Boocock, C., Van Straten, O.J., 1962. Notes on the geology and hydrogeology of the central Kalahari region, Bechuanaland Protectorate. South African Journal of Geology, 65(1), 125-176.

Botha, G.A., 2000. Paleosols and duricrusts. In: Partridge, T.C. and Maud, R.M. (Eds.) Cenozoic of Southern Africa. Oxford University Press, New York, Oxford Monographs on Geology and Geophysics, 40, pp.131-144,

Brook, G.A., Cowart, J.B., Brandt, S.A., 1998. Comparison of Quaternary environmental change in eastern and southern Africa using cave speleothem, tufa and rock shelter sediment data. In: Alsharhan, G., Whittle, Kendall (Eds.), Quaternary Deserts and Climate Change. Balkema, Rotterdam, pp. 239–250.

Brook, G.A., Scott, L. Railsback, L.B., Goddard, E.A., 2010. A 35 ka pollen and isotope record of environmental change along the southern margin of the Kalahari from a stalagmite and animal dung deposits in Wonderwerk Cave, South Africa. Journal of Arid Environments, 74, 870-884.

Bullard, J.E., Nash, D.J., 1998. Linear dune pattern variability in the vicinity of dry valleys in the south-west Kalahari. Geomorphology, 23, 35-54.

Bullard, J.E., Nash, D.J., 2000. Valley-marginal sand dunes in the south-west Kalahari: their nature, classification and possible origins. Journal of Arid Environments, 45, 369-383.

Bullard, J.E., Thomas, D.S.G., Livingstone, I., Wiggs, G.F.S., 1995. Analysis of linear sand dune morphological variability, southwestern Kalahari dunefield. Geomorphology, 11, 189-203.

Bultot, F., Griffiths, J.W., 1972. The equatorial wet zone. In: Griffiths, J.W. (Ed.), Climates of Africa. Elsevier, Amsterdam, World Survey of Climatology, vol. 10, pp. 259–311.

Burrough, S.L., Thomas, D.S.G., 2008. Late Quaternary lake-level fluctuations in the Mababe Depression: Middle Kalahari palaeolakes and the role of Zambezi inflows. Quaternary Research, 69, 388–403.

Burrough, S.L., Thomas, D.S., Bailey, R.M., 2009a. Mega-Lake in the Kalahari: a Late Pleistocene record of the Palaeolake Makgadikgadi system. Quaternary Science Reviews, 28(15-16), 1392-1411.

Burrough, S.L., Thomas, D.S., Singarayer, J.S., 2009b. Late Quaternary hydrological dynamics in the Middle Kalahari: forcing and feedbacks. Earth-Science Reviews, 96(4), 313-326.

Burrough, S.L., Thomas, D.S.G., Barham, L.S., 2019. Implications of a new chronology for the interpretation of the Middle and Later Stone Age of the upper Zambezi Valley. Journal of Archaeological Science: Reports, 23, 376-389.

Caracciolo, L., 2020. Sediment generation and sediment routing systems from a quantitative provenance analysis perspective: Review, application and future development. Earth-Science Reviews, 209, 103226.

Catuneanu, O., Wopfner, H., Eriksson, P.G., Cairncross, B., Rubidge, B.S., Smith, R.M.H., Hancox, P.J., 2005. The Karoo basins of south-central Africa. Journal of Asian Earth Sciences, 43, 211-253.

Chanvry, E., Ando, S., Garzanti, E., Guillocheau, F., Dall'Asta, M., Beaufort, D., Patrier, P., 2018. Impact of hinterland evolution in mineralogy of clastics sediments: first results from mineralogical analysis focus on the Zambezi system during Meso-Cenozoic times. EGU General Assembly Conference Abstracts, p. 18077.

Comas-Cufí, M., Thió-Henestrosa, F.S., CoDaPack 2.0: a stand-alone, multi-platform compositional software.

Cook, K., 2000. The South Indian convergence zone and interrannual rainfall variability over southern Africa. Journal of Climate, 13, 3789–3804.

Crouvi, O., Amit, R., Enzel, Y., Gillespie, A.R., 2010. Active sand seas and the formation of desert loess. Quaternary Science Reviews, 29(17-18), 2087-2098.

De Carvalho, H., Tassinari, C., Alves, P.H., Guimarães, F., Simões,M.C., 2000. Geochronological review of the Precambrian in western Angola: links with Brazil. Journal of African Earth Sciences, 31, 383–402.

De Ploey, J., Lepersonne, J., Stopps, G., 1968. Sédimentologie et origine de sables de la Série des "Grès polymorphes"(Système du Kalahari) au Congo occidental. Musée royal de L'Afrique Centrale Tervuren, Belqique, 61, 72 p.

De Wit, M., 2007. The Kalahari Epeirogeny and climate change: differentiating cause and effect from core to space. South African Journal of Geology, 110(2-3), 367-392.

Dirks, P.H.G.M., Blenkinsop, T.G., Jelsma, H.A., 2009. The Geological Evolution of Africa. In: De Vito, B., Grasemann, B., Stuwe, K. (Eds.), Geology. Encylopedia of Life Support Systems, vol. IV., EOLSS Publishers, Paris, 978-1-84826-457-1, pp. 230-251.

Du Toit, A.L., 1954. Geology of South Africa. Oliver & Boyd, London, 611 p.

East, A.E., Clift, P.D., Carter, A., Alizai, A., Van Laningham, S., 2015. Fluvial-eolian interactions in sediment routing and sedimentary signal buffering: an example from the Indus Basin and Thar Desert. Journal of Sedimentary Research, 85, 715-728.

Eglinger, A., Vanderhaeghe, O., André-Mayer, A.S., Goncalves, P., Zeh, A., Durand, C., Deloule, E., 2016. Tectono-metamorphic evolution of the internal zone of the Pan-African Lufilian orogenic belt (Zambia): Implications for crustal reworking and syn-orogenic uranium mineralizations. Lithos, 240, 167-188.

Eglington, B.M. 2006. Evolution of the Namaqua–Natal Belt, southern Africa—a geochronological and isotope geochemical review. Journal of African Earth Sciences, 46, 93-111.

Eglington, B.M., Armstrong, R.A. 2004. The Kaapvaal Craton and adjacent orogens, Southern Africa: a geochronological database and overview of the geological development of the craton. South African Journal of Geology, 107, 13-32.

Feller, W., 1948. On the Kolmogorov-Smirnov limit theorems for empirical distributions. Annals of Mathematical Statistics, 19, 177-189.

Frimmel, H.E., Basei, M.S., Gaucher, C. 2011. Neoproterozoic geodynamic evolution of SW-Gondwana: a southern African perspective. International Journal of Earth Sciences, 100, 323-354.

Gabriel, K.R., 1971. The biplot graphic display of matrices with application to principal component analysis. Biometrika, 58, 453-467.

Galehouse, J.S., 1971. Point counting. In: Carver, R.E. (Ed.), Procedures in sedimentary petrology. Wiley, New York, pp. 385-407.

Gärtner, A., Linnemann, U., Hofmann, M., 2014. The provenance of northern Kalahari Basin sediments and growth history of the southern Congo Craton reconstructed by U–Pb ages of zircons from recent river sands. International Journal of Earth Sciences, 103(2), 579-595.

Garzanti, E., 2016. From static to dynamic provenance analysis – Sedimentary petrology upgraded. In: Caracciolo, L., Garzanti, E., von Eynatten, H., Weltje, G.J. (Eds.), Sediment generation and provenance: processes and pathways. Sedimentary Geology, 336, 3-13.

Garzanti E., 2017. The maturity myth in sedimentology and provenance analysis. Journal of Sedimentary Research, 87, 353-365.

Garzanti, E., 2019. Petrographic classification of sand and sandstone. Earth-Science Reviews, 192, 545-563.

Garzanti, E., Andò, S., 2007. Heavy-mineral concentration in modern sands: implications for provenance interpretation. In: Mange, M.A., Wright, D.T. (Eds.), Heavy minerals in use. Elsevier, Amsterdam, Developments in Sedimentology Series, 58, pp. 517-545.

Garzanti, E., Andò, S., 2019. Heavy Minerals for Junior Woodchucks. Minerals, 9(3), 148, doi:10.3390/min9030148.

Garzanti, E., Vezzoli, G. 2003. A classification of metamorphic grains in sands based on their composition and grade. Journal of Sedimentary Research, 73, 830-837.

Garzanti, E., Vezzoli, G., Ando, S., Castiglioni, G., 2001. Petrology of rifted-margin sand (Red Sea and Gulf of Aden, Yemen). The Journal of Geology, 109(3), 277-297.

Garzanti, E., Ando, S., Vezzoli, G., Dell'Era, D., 2003. From rifted margins to foreland basins: investigating provenance and sediment dispersal across desert Arabia (Oman, UAE). Journal of Sedimentary Research, 73(4), 572-588.

Garzanti, E., Ando, S., Vezzoli, G., 2006. The continental crust as a source of sand (southern Alps cross section, northern Italy). The Journal of Geology, 114(5), 533-554.

Garzanti, E., Resentini, A., Vezzoli, G., Ando, S., Malusa, M.G., Padoan, M., Paparella, P., 2010. Detrital fingerprints of fossil continental-subduction zones (Axial Belt Provenance, European Alps). The Journal of Geology, 118(4), 341-362.

Garzanti, E., Andò, S., Vezzoli, G., Lustrino, M., Boni, M., Vermeesch, P., 2012. Petrology of the Namib sand sea: long-distance transport and compositional variability in the wind-displaced Orange Delta. Earth-Science Reviews, 11, 173-189.

Garzanti, E., Vermeesch, P., Andò, S., Vezzoli, G., Valagussa, M., Allen, K., Kadi, K.A., Al-Juboury, A.I., 2013. Provenance and recycling of Arabian desert sand. Earth-Science Reviews, 120, 1-19.

Garzanti, E., Vermeesch, P., Padoan, M., Resentini, A., Vezzoli, G., Andò, S., 2014a. Provenance of passive-margin sand (southern Africa). The Journal of Geology, 122, 17-42.

Garzanti, E., Padoan, M., Setti, M., López-Galindo, A., Villa, I.M., 2014b. Provenance versus weathering control on the composition of tropical river mud (southern Africa). Chemical Geology, 366, 61-74.

Garzanti, E., Andò, S., Padoan, M., Vezzoli, G., El Kammar, A., 2015a. The modern Nile sediment system: Processes and products. Quaternary Science Reviews, 130, 9-56.

Garzanti, E., Resentini, A., Andò, S., Vezzoli, G., Vermeesch, P., 2015b. Physical controls on sand composition and relative durability of detrital minerals during long-distance littoral and eolian transport (coastal Namibia). Sedimentology, 62, 971-996.

Garzanti, E., Vermeesch, P., Al-Ramadan, K.A., Andò, S., Limonta, M., Rittner, M., Vezzoli, G., 2017. Tracing transcontinental sand transport: from Anatolia–Zagros to the Rub'Al Khali Sand Sea. Journal of Sedimentary Research, 87(11), 1196-1213.

Garzanti, E., Dinis, P., Vermeesch, P., Andò, S., Hahn, A., Huvi, J., Limonta, M., Padoan, M., Resentini, A., Rittner, M., Vezzoli, G., 2018a. Dynamic uplift, recycling, and climate control on the petrology of passive-margin sand (Angola). Sedimentary Geology, 375, 86-104.

Garzanti, E., Vermeesch, P., Rittner, M., Simmons, M., 2018b. The zircon story of the Nile: Time- structure maps of source rocks and discontinuous propagation of detrital signals. Basin Research, 30, 1098-1117.

Garzanti, E., Ghassemi, M.R., Limonta, M., Resentini, A., 2019a. Provenance of Karakum Desert sand (Turkmenistan): lithic-rich orogenic signature of central Asian dune fields. Rivista Italiana di Paleontologia e Stratigrafia, 125(1), 77-89.

Garzanti, E., Vermeesch, P., Vezzoli, G., Andò, S., Botti, E., Limonta, M., Dinis, P., Hahn, A., Baudet, D., De Grave, J., Yaya, N.K., 2019b. Congo River sand and the equatorial quartz factory. Earth-Science Reviews, 197, 102918.

Garzanti, E., Liang, W., Andò, S., Clift, P.D., Resentini, A., Vermeesch, P., Vezzoli, G., 2020. Provenance of Thal Desert sand: Focused erosion in the western Himalayan syntaxis and foreland-basin deposition driven by latest Quaternary climate change. Earth-Science Reviews, 207, 103220.

Garzanti, E., Pastore, G., Resentini, A., Vezzoli, G., Vermeesch, P., Ngube, L., Van Niekerk, E., Jouet, G., Dall'Asta, M., 2021a. The segmented Zambezi sedimentary system from source to sink 1. Sand petrology and heavy minerals. The Journal of Geology, 129(4), 343-369.

Garzanti, E., Capaldi, T., Vezzoli, G., Limonta, M., Vezzoli, G., Sosa, N., 2021b. Transcontinental retroarc sediment routing controlled by subduction geometry and climate change (Central and Southern Andes, Argentina). Basin Research, https://doi.org/10.1111/bre.12607 (32 p.).

Geyh, M.A., Eitel, B., 1997. Radiometric dating of young and old calcrete. Radiocarbon 40(2), 795–802,

Glynn, S.M., Master, S., Frei, D., Wiedenbeck, M., 2020. U-Pb zircon geochronology of the Dete-Kamativi Inlier, NW Zimbabwe, with implications for the western margin of the Archaean Zimbabwe Craton. Precambrian Research, 346, 105824.

Goscombe, B., Foster, D.A., Gray, D., Wade, B., 2020. Assembly of central Gondwana along the Zambezi Belt: Metamorphic response and basement reactivation during the Kuunga Orogeny. Gondwana Research, 80, 410-465.

Goudie, A.S., 2020. Duricrusts and landforms. In: Richards, K.S., Arnett, R.R., Ellis. S. (Eds.), Geomorphology and soils. Routledge, Milton Park (UK), ch. 2, pp. 37-57.

Goudie, A.S., Middleton, N.J., 2006. Desert dust in the global system. Springer Science & Business Media. Berlin, 286 p.

Goudie A.S., Thomas, D.S.G., 1985. Pans in southern Africa with particular reference to South Africa and Zimbabwe. Zeitschrift für Geomorphologie N.F., 29(1), 1-19.

Goudie, A., Viles, H., 2015. Landscapes and Landforms of Namibia. Springer Netherlands, 173 p.

Greber, N.D., Davies, J.H., Gaynor, S.P., Jourdan, F., Bertrand, H., Schaltegger, U., 2020. New high precision U-Pb ages and Hf isotope data from the Karoo large igneous province; implications for pulsed magmatism and early Toarcian environmental perturbations. Results in Geochemistry, 1, 100005.

Griffin, W.L., Powell, W.J., Pearson, N.J., O'Reilly, S.Y., 2008. GLITTER: data reduction software for laser ablation ICP-MS. Laser Ablation-ICP-MS in the earth sciences. Mineralogical association of Canada short course series, 40, 204-207.

Gumbricht, T., McCarthy, T.S., Merry, C.L., 2001. The topography of the Okavango Delta, Botswana, and its tectonic and sedimentological implications. South African Journal of Geology, 104(3), 243-264.

Haddon, I.G., 2005. The sub-Kalahari geology and tectonic evolution of the Kalahari Basin, southern Africa. Unpublished Ph. D. thesis, University of the Witwatersrand, Johannesburg, 346 p.

Haddon, I.G., McCarthy, T.S., 2005. The Mesozoic–Cenozoic interior sag basins of Central Africa: the Late-Cretaceous–Cenozoic Kalahari and Okavango basins. Journal of African Earth Sciences, 43, 316-333.

Hall, W.S., Hitzman, M.W., Kuiper, Y.D., Kylander-Clark, A.R., Holm-Denoma, C.S., Moscati, R.J., Plink-Björklund, P., Enders, M.S., 2018. Igneous and detrital zircon U-Pb and Lu-Hf geochronology of the late Meso-to Neoproterozoic northwest Botswana rift: Maximum depositional age and provenance of the Ghanzi Group, Kalahari Copperbelt, Botswana and Namibia. Precambrian Research, 318, 133-155.

Hanson, R.E. 2003. Proterozoic geochronology and tectonic evolution of southern Africa. In: Yoshida, M.; Windley, B.F.; and Dasgupta, S. eds. Proterozoic East Gondwana: supercontinent assembly and breakup. Geological Society, London, Special Publications, 206, 427-463.

Hanson, R.E., Harmer, R.E., Blenkinsop, T.G., Bullen, D.S., Dalziel, I.W.D., Gose,W.A., Hall, R.P., Kampunzu, A.B., Key, R.M., Mukwakwami, J., Munyanyiwa, H., Pancake, J.A., Seidel, E.K.,Ward, S.E., 2006. Mesoproterozoic intraplate magmatism in the Kalahari Craton: a review. Journal of African Earth Sciences, 46, 141-167.

Hargrove, U.S., Hanson, R.E., Martin, M.W., Blenkinsop, T.G., Bowring, S.A., Walker, N., Munyanyiwa, H., 2003. Tectonic evolution of the Zambezi orogenic belt: geochronological, structural, and petrological constraints from northern Zimbabwe. Precambrian Research, 123(2-4), 159-186.

Hay, W.W., 1998. Detrital sediment fluxes from continents to oceans. Chemical geology, 145(3-4), 287-323.

Hipondoka, M.H.T., Mauz, B., Kempf, J., Packman, S., Chiverrell, R.C., Bloemendal, J., 2014. Chronology of sand ridges and the Late Quaternary evolution of Etosha Pan, Namibia. Geomorphology, 204, 553-563.

Holisticos, 2012. Environmental Impact Study for the Rehabilitation and Expansion of the Cambambe Hydroelectric Power Plant. https://www.miga.org/documents/Angola_ Cambambe_HPP_EIS.pdf.

Holmgren, K., Karlén, W., Shaw, P. A., 1995. Paleoclimatic significance of the stable isotopic composition and petrology of a Late Pleistocene stalagmite from Botswana. Quaternary Research, 32, 320-328.

Holmgren, K., Lee-Thorp, J.A., Cooper, G.R., Lundblad, K., Partridge, T.C., Scott, L., Sithaldeen, R., Talma, A.S., Tyson, P.D., 2003. Persistent millennial-scale climatic variability over the past 25,000 years in Southern Africa. Quaternary Science Reviews, 22(21-22), 2311-2326.

Holzkämper, S., Holmgren, K., Lee-Thorp, J. L., Talma, S., Mangini, A., Partridge, T., 2009. Late Pleistocene stalagmite growth in Wolkberg Cave, South Africa. Earth and Planetary Science Letters, 282, 212-221.

Houben, G.J., Kaufhold, S., Miller, R.M., Lohe, C., Hinderer, M., Noll, M., Hornung, J., Joseph, R., Gerdes, A., Sitnikova, M., Quinger, M., 2020. Stacked megafans of the Kalahari Basin as archives of paleogeography, river capture, and Cenozoic paleoclimate of southwestern Africa. Journal of Sedimentary Research, 90(9), 980-1010.

Hubert, J.F., 1962. A zircon–tourmaline–rutile maturity index and the interdependence of the composition of heavy mineral assemblages with the gross composition and texture of sandstones. Journal of Sedimentary Petrology, 32, 440-450.

Huntsman-Mapila, P., Kampunzu, A.B., Vink, B., Ringrose, S., 2005. Cryptic indicators of provenance from the geochemistry of the Okavango Delta sediments, Botswana. Sedimentary Geology, 174(1-2), 123-148.

Hürkamp, K., Völkel, J., Heine, K., Bens, O., Leopold, M., Winkelbauer, J., 2011. Late Quaternary environmental changes from aeolian and fluvial geoarchives in the southwestern Kalahari, South Africa: implications for past African climate dynamics. South African Journal of Geology, 114 (3–4), 459–474.

Ingersoll, R.V., Bullard, T.F., Ford, R.L., Grimm, J.P., Pickle, J.D., Sares, S.W., 1984. The effect of grain size on detrital modes: a test of the Gazzi-Dickinson point-counting method. Journal of Sedimentary Petrology, 54, 103-116.

Inman, D.L., Jenkins, S.A., 1984. The Nile littoral cell and man's impact on the coastal zone of the southeastern Mediterranean. Coastal Engineering, ch. 109, 1600-1617.

Jackson, S.E., Pearson, N.J., Griffin, W.L., Belousova, E.A., 2004. The application of laser ablation-inductively coupled plasma-mass spectrometry to in situ U–Pb zircon geochronology. Chemical Geology, 211, 47-69.

Jacobs, J., Pisarevsky, S., Thomas, R.J., Becker, T. 2008. The Kalahari Craton during the assembly and dispersal of Rodinia. Precambrian Research, 160, 142-158.

Jelsma, H.A., Dirks, P.H.G.M., 2002. Neoarchaean tectonic evolution of the Zimbabwe Craton. In: Fowler, C. M.R., Ebinger, C.J., Hawkesworth, C.J. (Eds), The early Earth: physical, chemical and biological development. Geological Society London, Special Publication 199, 183-211.

Jelsma, H.A., McCourt, S., Perritt, S.H., Armstrong R.A., 2018. The Geology and Evolution of the Angolan Shield, Congo Craton. In Siegesmund, S., Basei, M., Oyhantçabal, P., Oriolo, S. (Eds.), Geology of Southwest Gondwana. Regional Geology Reviews. Springer, Cham, pp. 217-239. https://doi.org/10.1007/978-3-319-68920-3_9.

John, T., Schenk, V., Mezger, K., Tembo, F., 2004. Timing and PT evolution of whiteschist metamorphism in the Lufilian Arc–Zambezi Belt orogen (Zambia): implications for the assembly of Gondwana. The Journal of Geology, 112(1), 71-90.

Johnson, M.R., 1991. Sandstone petrography, provenance and plate tectonic setting in Gondwana context of the southeastern Cape-Karoo Basin. South African Journal of Geology, 94(2), 137-154.

Johnson, M.R., van Vuuren, C.J., Hegenberger, W.F., Key, R.,Shoko, U. 1996. Stratigraphy in the Karoo Supergroup in southern Africa: an overview. Journal of African Earth Sciences, 23, 3-15.

Jung, S., Hoffer, E., Hoernes, S., 2007. Neo-Proterozoic rift-related syenites (Northern Damara Belt, Namibia): Geochemical and Nd–Sr–Pb–O isotope constraints for mantle sources and petrogenesis. Lithos, 96, 415-435.

Kampunzu, A.B., Cailteux, J., 1999. Tectonic evolution of the Lufilian Arc (Central Africa Copper Belt) during Neoproterozoic Pan African orogenesis. Gondwana Research, 2(3), 401-421.

Kampunzu, A.B., Ringrose, S., Huntsman-Mapila, P., Harris, C., Vink, B. W., Matheson, W., 2007. Origins and palaeo-environments of Kalahari duricrusts in the Moshaweng dry valleys (Botswana) as detected by major and trace element composition. Journal of African Earth Sciences, 48(2-3), 199-221.

Kinabo, B.D., Atakwana, E.A., Hogan, J.P., Modisi, M.P., Wheaton, D.D., Kampunzu, A.B., 2007. Early structural development of the Okavango rift zone, NW Botswana. Journal of African Earth Sciences, 48, 125–136.

Kiss, T., Sipos, G., Kovács, F., 2009. Human impact on fixed sand dunes revealed by morphometric analysis. Earth Surface Processes and Landforms. 34(5), 700-711.

Klöcking M., Hoggard, M.J., Tribaldos, V.R., Richards, F.D., Guimarães, A.R., Maclennan, J., White, N.J., 2020. A tale of two domes: Neogene to recent volcanism and dynamic uplift of northeast Brazil and southwest Africa. Earth and Planetary Science Letters, 547, 116464.

Kottek, M., Grieser, J., Beck, C., Rudolf, B., Rubel, F., 2006. World map of the Köppen–Geiger climate classification updated. Meteorologische Zeitschrift, 15, 259–263.

Kruskal, J.B., Wish, M., 1978. Multidimensional scaling. Sage Publications, Newbury Park (CA), Quantitative applications in the social sciences, Sage University Paper Series 07-011, 92 p.

Kulongoski, J.T., Hilton, D.R., Selaolo, E.T., 2004. Climate variability in the Botswana Kalahari from the late Pleistocene to the present day. Geophysical Research Letters, 31, L10204.

Kusky, T.M. 1998. Tectonic setting and terrane accretion of the Archean Zimbabwe craton. Geology, 26, 163-166.

Lancaster, N., 1978. The Pans of the southern Kalahari, Botswana. The Geographical Journal, 144, 81-98.

Lancaster, N., 1979. Quaternary environments in the arid zone of southern Africa, Dept. Geogr. and Envir. Studies, Occ. Pap. 22, pp. 73, Univ. Witswatersrand, Johannesburg

Lancaster, N., 1981. Paleoenvironmental implications of fixed dune systems in southern Africa. Palaeogeography, Palaeoclimatology, Palaeoecology, 33(4), 327-346.

Lancaster, N., 1986. Pans in the southwestern Kalahari: a preliminary report. In: Southern African society for Quaternary research. Biennal conference, 7, pp. 59-67.

Lanci, L., Tohver, E., Wilson, A., Flint, S., 2013. Upper Permian magnetic stratigraphy of the lower Beaufort group, Karoo basin. Earth and Planetary Science Letters, 375, 123-134.

Lehmann, J., Saalmann, K., Naydenov, K.V., Milani, L., Belyanin, G.A., Zwingmann, H., Charlesworth, G., Kinnaird, J.A., 2016. Structural and geochronological constraints on the Pan- African tectonic evolution of the northern Damara Belt, Namibia. Tectonics, 35(1), 103-135.

Ludwig, K.R., 1998. On the treatment of concordant uranium-lead ages. Geochimica et Cosmochimica Acta, 62, 665-676.

Lukich, V., Porat, N., Faershtein, G., Cowling, S., Chazan, M., 2019. New chronology and stratigraphy for Kathu Pan 6, South Africa. Journal of Palaeolithic Archaeology, 2, 235-257.

Lukich, V., Cowling, S., Chazan, M., 2020. Palaeoenvironmental reconstruction of Kathu Pan, South Africa, based on sedimentological data. Quaternary Science Reviews, 230, 106153.

Lutjeharms, J.R.E., Van Ballegooyen, R.C., 1988. The retroflection of the Agulhas Current. Journal of Physical Oceanography, 18(11), 1570-1583.

Mange, A., Maurer, H.F.W., 1992. Heavy Minerals in Colour. Chapman and Hall, London, 147 p.

Matmon, A., Hidy, A.J., Vainer, S., Crouvi, O., Fink, D., Erel, Y., Arnold, M., Aumaître, G., Bourlès, D., Keddadouche, K., Horwitz, L.K., Chazan, M., 2015. New chronology for the southern Kalahari Group sediments with implications for sediment-cycle dynamics and early hominin occupation. Quaternary Research, 84, 118-132.

Matmon, A., Enzel, Y., Vainer, S., Grodek, T., Mushkin, A., and ASTER Team, 2018. The near steady state landscape of western Namibia. Geomorphology, 313, 72-87.

Mayaud, J.R., Bailey, R.M., Wiggs, G.F., 2017. Modelled responses of the Kalahari Desert to 21st century climate and land use change. Scientific reports, 7(1), 3887, doi:10.1038/s41598-017-04341-0.

McCarthy, T.S., Ellery, W.N., 1995. Sedimentation on the distal reaches of the Okavango Fan, Botswana, and its bearing on calcrete and silcrete (ganister) formation. Journal of Sedimentary Research, 65(1a), 77-90.

McCarthy, T.S., Ellery, W.N., 1998. The Okavango delta. Transactions of the Royal Society of South Africa, 53(2), 157-182.

McCarthy, T.S., Metcalfe, J., 1990. Chemical sedimentation in the semi-arid environment of the Okavango Delta, Botswana. Chemical Geology, 89, 157–178.

McCarthy, T.S., Humphries, M.S., Mahomed, I., Le Roux, P., Verhagen, B.T., 2012. Island forming processes in the Okavango Delta, Botswana. Geomorphology, 179, 249-257.

McCourt, S., Armstrong, R.A., Jelsma, H., Mapeo, R.B.M., 2013. New U–Pb SHRIMP ages from the Lubango region, SW Angola: insights into the Palaeoproterozoic evolution of the Angolan Shield, southern Congo Craton, Africa. Journal of the Geological Society London, 170, 353–363.

McFarlane, M.J., Eckardt, F.D., 2007. Palaeodune morphology associated with the Gumare fault of the Okavango graben in the Botswana/Namibia borderland: a new model of tectonic influence. South African Journal of Geology, 110(4), 535-542.

McFarlane, M.J., Long, C.W., 2015. Pan floor 'barchan'mounds, Ntwetwe Pan, Makgadikgadi, Botswana: Their origin and palaeoclimatic implications. Quaternary International, 372, 108-119.

McFarlane, M.J., Segadika, P., 2001. Archaeological evidence for the reassessment of the ages of the Makgadikgadi paleolakes. Botswana Notes & Records, 33(1), 83-89.

McFarlane, M.J., Eckardt, F.D., Ringrose, S., Coetzee, S.H., Kuhn, J.R., 2005. Degradation of linear dunes in Northwest Ngamiland, Botswana and the implications for luminescence dating of periods of aridity. Quaternary International, 135(1), 83-90.

McFarlane, M.J., Eckardt, F.D., Coetzee, S.H., Ringrose, S., 2010. An African surface weathering profile in the Kalahari of North West Ngamiland, Botswana: processes and products. Zeitschrift für Geomorphologie, 54(3), 273-303.

McKay, M.P., Coble, M.A., Hessler, A.M., Weislogel, A.L., Fildani, A., 2016. Petrogenesis and provenance of distal volcanic tuffs from the Permian–Triassic Karoo Basin, South Africa: A window into a dissected magmatic province. Geosphere, 12(1), 1-14.

Miller, R.M. 2008, The geology of Namibia. Ministry of Mines and Energy, Windhoek (3 vol.).

Miller, R.M., 2014. Evidence for the evolution of the Kalahari dunes from the Auob River, southeastern Namibia. Transactions of the Royal Society of South Africa, 69(3), 195-204.

Miller, R.M., Pickford, M., Senut, B., 2010. The geology, palaeontology and evolution of the Etosha Pan, Namibia: Implications for terminal Kalahari deposition. South African Journal of Geology, 113(3), 307-334.

Modisi, M.P., Atekwana, E.A., Kampunzu, A.B., Ngwisanyi, T.H., 2000. Rift kinematics during the incipient stages of continental extension: Evidence from the nascent Okavango rift basin, northwest Botswana. Geology, 28(10), 939-942.

Moore, A.E., Dingle, R.V., 1998. Evidence for fluvial sediment transport of Kalahari sands in central Botswana. South African Journal of Geology, 101(2), 143-153.

Moore, A.E., Larkin, P.A., 2001. Drainage evolution in south-central Africa since the breakup of Gondwana. South African Journal of Geology, 104, 47-68.

Moore, A.E., Cotterill, F., Main, M.P.L., Williams, H.B., 2007. The Zambesi River. In: Gupta, A. (Ed.), Large Rivers: Geomorphology and Management. Chichester, Wiley, pp. 311-332.

Moore, A.E., Blenkinsop, T., Cotterill, F., 2008. Controls on post-Gondwana alkaline volcanism in Southern Africa. Earth and Planetary Science Letters, 268(1-2), 151-164.

Moore, A.E., Cotterill, F.P.D., Eckardt, F.D., 2012. The evolution and ages of Makgadikgadi palaeo-lakes: consilient evidence from Kalahari drainage evolution south-central Africa. South African Journal of Geology, 115(3), 385-413.

Moucha, R., Forte, A.M. 2011. Changes in African topography driven by mantle convection. Nature Geosciences, 4, 707-712.

Nash, D.J., 2015. Of dunes, depressions and dry valleys: the arid landscapes of the Kalahari desert. In: Grab, S., Knight, J. (Eds.), Landscapes and Landforms of South Africa. Springer, Berlin, pp.129-137.

Nash, D.J., Endfield, G.H., 2002. Historical flows in the dry valleys of the Kalahari identified from missionary correspondence. South African Journal of Science, 98, 244–248.

Nash, D.J., Shaw, PA., 1998. Silica and carbonate relationships in silcrete-calcrete intergrade duricrusts from the Kalahari desert of Botswana and Namibia. Journal of African Earth Sciences, 27, 11–25.

Nash, D.J., McLaren, S.J., 2003. Kalahari valley calcretes: their nature, origins, and environmental significance. Quaternary International, 111(1), 3-22.

Nash, D.J., McLaren, S.J., Webb, J.A., 2004. Petrology, geochemistry and environmental significance of silcrete- calcrete intergrade duricrusts at Kang Pan and Tswaane, central Kalahari, Botswana. Earth Surface Processes and Landforms, 29(12), 1559-1586.

Nesbitt, H.W., Young, G.M., 1982. Early Proterozoic climates and plate motions inferred from major element chemistry of lutites. Nature, 299, 715-717.

Nicholson, S.E., 1996. A review of climate dynamics and climate variability in eastern Africa. In: Johnson, T.C., Odada, E.O. (Eds.), The Limnology, Climatology and Palaeoclimatology of the East African Lakes. Gordon and Breach, Amsterdam, pp. 25–56.

Nikulin, G., Hewitson, B., 2019. A simple set of indices describing the Tropical Rain Belt over central and southern Africa. Atmospheric Science Letters, 20(12), e946.

O'Connor, P.W., Thomas, D.S.G., 1999. The timing and environmental significance of Late Quaternary linear dune development in western Zambia. Quaternary Research, 52, 44-55.

Parker, A. 1970. An index of weathering for silicate rocks. Geological Magazine, 107, 501-504.

Partridge, T.C., 1993. The evidence for Cainozoic aridification in southern Africa. Quaternary International, 17, 105-110.

Pastore, G., Baird, T., Vermeesch, P., Resentini, A., Garzanti, E., 2021. Provenance and recycling of Sahara Desert sand. Earth-Science Reviews, 216, 103606.

Pickering, R., Hanock, P. J., Lee-Thopr, J.A., Grün, R., Mortimer, G.E., McCulloch, M., Berger, L.R., 2007. Stratigraphy, U-Th chronology, and paleoenvironments at Gladysvale Cave: insights into the climatic control of South African hominin-bearing cave deposits. Journal of Human Evolution, 53, 602-619.

Poldervaart, A., 1957. Kalahari sands. In: Clark, J.D. (Ed.), The 3rd Pan-African Congress on Prehistory, Livingstone 1955. Chatto & Windus, London, pp. 106–119.

Reason, C.J.C., 2001. Evidence for the influence of the Agulhas current on regional atmospheric circulation patterns. Journal of Climate, 14, 2769–2778.

Resentini, A., Andò, S., Garzanti, E., 2018. Quantifying roundness of detrital minerals by image analysis: Sediment transport, shape effects, and provenance implications. Journal of Sedimentary Research, 88(2), 276-289.

Ringrose, S., Kampunzu, A.B., Vink, B.W., Matheson, W., Downey, W.S., 2002. Origin and palaeo- environments of calcareous sediments in the Moshaweng dry valley, southeast Botswana. Earth Surface Processes and Landforms, 27(6), 591-611.

Ringrose, S., Harris, C., Huntsman-Mapila, P., Vink, B.W., Diskins, S., Vanderpost, C., Matheson, W., 2009. Origins of strandline duricrusts around the Makgadikgadi Pans (Botswana Kalahari) as deduced from their chemical and isotope composition. Sedimentary Geology, 219(1-4), 262-279.

Rittner, M., Vermeesch, P., Carter, A., Bird, A., Stevens, T., Garzanti, E., Andò, S., Vezzoli, G., Dutt, R., Xu, Z., Lu, H., 2016. The provenance of Taklamakan desert sand. Earth and Planetary Science Letters, 437, 127-137.

Rogers, J., Bremner, J.M., 1991. The Benguela Ecosystem. Part VII. Marine-geological aspects. In: Barnes, M. (Ed.), Oceanography and marine biology, an annual review, vol. 29. Aberdeen University Press, pp. 1–86.

Romans, B.W., Castelltort, S., Covault, J.A., Fildani, A., Walsh, J.P., 2016. Environmental signal propagation in sedimentary systems across timescales. Earth-Science Reviews, 153, 7-29.

Schlegel, G.C.J., von Harmse, H.J.M., Brunke, O., 1989. Granulometric and mineralogical characteristics of the Kalahari sands of southern Africa. South African Journal of Geology, 92(3), 207-222.

Schlüter, T. 2008. Geological Atlas of Africa. Springer, Heidelberg, 307 p.

Schüller, I., Blez, L., Wilkes, H., Wehrmann, A., 2018. Late Quaternary shift in southern African rainfall zones: sedimentary and geochemical data from Kalahari pans. Zeitschrift für Geomorphologie, 61(4), 339-362.

Schulze, B. (1972). South Africa. In: Griffiths, J.W. (Ed.), Climates of Africa. Elsevier, Amsterdam, World Survey of Climatology, vol. 10, pp. 501–586.

Shaw, P.A., de Vries, J.J., 1988. Duricrust, groundwater and valley development in the Kalahari of south-east Botswana. Journal of Arid Environments, 14, 245-254.

Shaw, A.I., Goudie, A.S., 2002. Geomorphological evidence for the extension of the Mega-Kalahari into south-central Angola. South African Geographical Journal, 84, 182-194.

Shaw, P.A., Nash, D.J., 1998. Dual mechanisms for the formation of fluvial silcretes in the distal reaches of the Okavango Delta Fan, Botswana. Earth Surface Processes and Landforms, 23(8), 705-714.

Shaw, P., Thomas, D.S.G. 1992. Geomorphology, sedimentation and tectonics in the Kalahari Rift. Israel Journal of Earth Sciences, 41, 87–94.

Shaw, P.A., Thomas, D.S.G., 1988. Lake Caprivi: a late Quaternary link between the Zambezi and middle Kalahari drainage systems. Zeitschrift für Geomorphologie, 32(3), 329-337.

Shaw, P.A., Thomas, D.S., Nash, D.J., 1992. Late Quaternary fluvial activity in the dry valleys (mekgacha) of the Middle and Southern Kalahari, southern Africa. Journal of Quaternary Science, 7(4), 273-281.

Sláma, J., Košler, J., Condon, D.J., Crowley, J.L., Gerdes, A., Hanchar, J.M., Horstwood, M.S., Morris, G.A., Nasdala, L., Norberg, N., Schaltegger, U., 2008. Plešovice zircon—a new natural reference material for U–Pb and Hf isotopic microanalysis. Chemical Geology, 249, 1-35.

Stokes, S., Haynes, G., Thomas, D.S.G., Horrocks, J.L., Higginson, M., Malifa, M., 1998. Punctuated aridity in southern Africa during the last glacial cycle: the chronology of linear dune construction in the northeastern Kalahari. Palaeogeography Palaeoclimatology Palaeoecology, 137, 305-322.

Stone, A., 2021a. Landscape evolution of the Stampriet Transboundary Basin and relation to the groundwater system: the land of duricrusts, pans, dry valleys and dunes, and the relation to the groundwater system. In Eckardt, F. (Ed.) Landscapes and Landforms of Botswana. Springer, Berlin, Part of the World Geomorphological Landscapes series, Springer Nature Switzerland, pp.9-10, ISBN/EAN 3030861015/9783030861018.

Stone, A., 2021b. Dryland dunes and other dryland environmental archives as proxies for Late Quaternary stratigraphy and environmental and climate change in southern Africa. South African Journal of Geology, doi:10.25131/sajg.124.0055.

Stone, A.E.C., Thomas, D.S.G., 2008. Linear dune accumulation chronologies from the southwest Kalahari, Namibia: challenges of reconstructing late Quaternary palaeoenvironments from aeolian landforms. Quaternary Science Reviews, 27(17-18), 1667-1681.

Stone, A., Bateman, M.D., Burrough, S.L., Garzanti, E., Limonta, M., Radeff, G., Telfer, M.W., 2019. Using a portable luminescence reader for rapid age assessment of aeolian sediments for reconstructing dunefield landscape evolution in southern Africa. Quaternary Geochronology, 49, 57-64.

Stute, M., Talma, A.S., 1998. Glacial temperatures and moisture transport regimes reconstructed from noble gases and δ^{18}O, Stampriet aquifer, Namibia. Isotope techniques in the study of environmental change. Proceedings of the International symposium on applications of isotope techniques in studying past and current environmental changes in the hydrosphere and the atmosphere, Vienna (Austria), 14/18 April 1997, 307-318.

Stuut, J.B., Smalley, I., O'Hara-Dhand, K., 2009. Aeolian dust in Europe: African sources and European deposits. Quaternary International, 198(1-2), 234-245.

Summerfield, M.A., 1983. Silcrete as a palaeoclimatic indicator: evidence from southern Africa Palaeogeography, Palaeoclimatology and Palaeoecology, 41, 65–79.

Svensen, H., Corfu, F., Polteau, S., Hammer, Ø., Planke, S., 2012. Rapid magma emplacement in the Karoo Large Igneous Province. Earth Planetary Science Letters, 325/326, 1-9.

Taylor, S.R., McLennan, S.M., 1995. The geochemical evolution of the continental crust. Reviews of Geophysics, 33, 241–265.

Telfer, M.W., Thomas, D.S.G., 2006. Complex Holocene lunette dune development, South Africa: Implications for palaeoclimate and models of pan development in arid regions. Geology, 34(10), 853-856.

Telfer, M.W., Thomas, D.S.G., Parker, A.G., Walkington, H., Finch, A.A., 2009. Optically Stimulated Luminescence (OSL) dating and palaeoenvironmental studies of pan (playa) sediment from Witpan, South Africa. Palaeogeography, Palaeoclimatology, Palaeoecology, 273, 50–60.

Thomas, D.S., 1984. Ancient ergs of the former arid zones of Zimbabwe, Zambia, and Angola. Transactions of the Institute of British Geographers, 9(1), 75-88.

Thomas, D.S.G., 1987. Discrimination of depositional environments using sedimentary characteristics in the Mega Kalahari, central southern Africa. In: Frostick, L., Reid, I. (Eds.), Desert Sediments: Ancient and Modern. Geological Society, London, Special Publications 35, pp. 293-306.

Thomas, D.S.G., Burrough, S.L., 2016. Luminescence-based chronologies in southern Africa: Analysis and interpretation of dune database records across the subcontinent. Quaternary International, 410(B), 30-45.

Thomas, D.S.G., Shaw, P.A. 1988. Late Cainozoic drainage evolution in the Zambezi basin: evidence from the Kalahari rim. Journal of African Earth Sciences, 7, 611-618.

Thomas, D.S.G., Shaw, P.A., 1990. The deposition and development of the Kalahari Group sediments, Central Southern Africa. Journal of African Earth Sciences (and the Middle East), 10(1-2), 187-197.

Thomas D.S.G., Shaw, P.A., 1991. The Kalahari Environment. Cambridge University Press, Cambridge, 287 p.

Thomas, D.S.G., Brook, G., Shaw, P., Bateman, M., Haberyan, K., Appleton, C., Nash, D., McLaren, S., Davies, F., 2003. Late Pleistocene wetting and drying in the NW Kalahari: an integrated study from the Tsodilo Hills, Botswana. Quaternary International, 104, 53–67.

Thomas, D.S., Knight, M., Wiggs, G.F., 2005. Remobilization of southern African desert dune systems by twenty-first century global warming. Nature, 435(7046), 1218-1221.

Todd, M.C., Washington, R., Palmer, P.I., 2002. Water vapour transport associated with tropical-temperate trough systems over southern Africa and the Southwest Indian Ocean. Journal of Climate, 24, 555–568.

Trumbull, R.B., Harris, C., Frindt, S., Wigand, M., 2004. Oxygen and neodymium isotope evidence for source diversity in Cretaceous anorogenic granites from Namibia and implications for A-type granite genesis. Lithos, 73, 21–40.

Tyson, S.J., 1999. Sand ramps or climbing dunes? Identification and palaeoenvironmental significance of aeolian deposits in the southern Kalahari and Breede River Valley, South Africa. MSc Dissertation, University of Cape Town, 136 p.

Tyson, P.D., Preston-Whyte, R.A., 2000. The Weather and Climate of Southern Africa, 2nd edition. Oxford University Press, Cape Town, 396 p.

Vainer, S., Ben Dor, Y., 2021. The Cosmolian program for simulating aeolian dynamics and its application to central Australia. Earth Surface Processes and Landforms, 46(9), 1631-1639.

Vainer, S., Erel, Y., Matmon, A., 2018a. Provenance and depositional environments of Quaternary sediments in the southern Kalahari Basin. Chemical Geology, 476, 352-369.

Vainer, S., Ben Dor, Y., Matmon, A., 2018b. Coupling cosmogenic nuclides and luminescence dating into a unified accumulation model of aeolian landforms age and dynamics: The case study of the Kalahari Erg. Quaternary Geochronology, 48, 133-144.

Vainer, S., Matmon, A., Dor, Y.B., Verrecchia, E., Aumaitre, G., 2021a. Eolian chronology reveals causal links between tectonics, climate, and erg generation. Nature Portfolio, doi:10.21203/rs.3.rs-801542/v1.

Vainer, S., Matmon, A., Erel, Y., Hidy, A.J., Crouvi, O., De Wit, M., Geller, Y., and ASTER Team, 2021b. Landscape responses to intraplate deformation in the Kalahari constrained by sediment provenance and chronology in the Okavango Basin. Basin Research, 33(2), 1170-1193.

Van Rensburg, H.J., 1971. Range ecology in Botswana. Vegetation studies in connection with vegetation/soil correlation and bush encroachment investigations. FAO Technical Document, nº 2, UNDP/SF/359/(BOT.1), Rome.

Van Veelen, M., Baker, T., Mulale, K., Bron, A., Fanta, A., Jonker, V., Mullins, W., Shoeman, H., 2009. Feasibility Study of the Potential for Sustainable Water Resources Development in the Molopo-Nossob Watercourse. ILISO Consulting LTD Project no 700192, 106 p.

Verboom, W.C., 1974. The Barotse loose sands of Western Province, Zambia. Zambian Geographical Magazine, 27, 13-17.

Vermeesch, P., 2012. On the visualisation of detrital age distributions. Chemical Geology, 312, 190-194.

Vermeesch, P., 2013. Multi-sample comparison of detrital age distributions. Chemical Geology, 341, 140-146.

Vermeesch, P., 2018. IsoplotR: A free and open toolbox for geochronology. Geoscience Frontiers, 9, 1479-1493.

Vermeesch, P., 2021. On the treatment of discordant detrital zircon U–Pb data. Geochronology Discussions, 1-19.

Vermeesch, P., Resentini, A., Garzanti, E., 2016. An R package for statistical provenance analysis. Sedimentary Geology, 336, 14-25.

Vermeesch, P., Rittner, M., Petrou, E., Omma, J., Mattinson, C, Garzanti, E., 2017. High throughput petrochronology and sedimentary provenance analysis by automated phase mapping and LAICPMS. Geochemistry, Geophysics, Geosystems, 18, doi:10.1002/2017GC007109.

Vigaud, N., Richard, Y., Rouault, M., Fauchereau, N., 2009. Moisture transport between the South Atlantic Ocean and southern Africa: relationships with summer rainfall and associated dynamics. Climate Dynamics, 32, 113-123.

Walker, N., 1990. Links between South African summer rainfall and temperature variability of the Agulhas and Benguela current systems. Journal of Geophysical Research, 95, 3297–3319.

Washington, R., Preston, A., 2006. Extreme wet years over southern Africa: role of Indian Ocean sea surface temperatures. Journal of Geophysical Research, 111, doi:10.1029/2005JD006724

Watts, N.L., 1980. Quaternary pedogenic calcretes from the Kalahari (southern Africa): mineralogy, genesis and diagenesis. Sedimentology, 27(6), 661-686.

White, K., Bullard, J., Livingstone, I., Moran, L., 2015. A morphometric comparison of the Namib and southwest Kalahari dunefields using ASTER GDEM data. Aeolian Reserch, 19, part A, 87-95.

Wiggs, G.F.S., Livingstone, I., Thomas, D.S.G., Bullard, J.E., 1995. Dune mobility and vegetation cover in the southwest Kalahari Desert. Earth Surface Processes Landforms, 20, 515-529.

Wiggs, G.F., Livingstone, I., Thomas, D.S., Bullard, J.E., 1996. Airflow and roughness characteristics over partially vegetated linear dunes in the southwest Kalahari Desert. Earth Surface Processes and Landforms, 21(1), 19-34.

Wilkins, J., Schoville, B.J., Pickering, R., Gliganic, L., Collins, B., Brown, K.S., von der Meden, J., Khumalo, W., Meyer, M.C., Maape, S., Blackwood, A.F., Hatton, A., 2021. Innovative Homo sapiens behaviours 105,000 years ago in a wetter Kalahari. Nature, 592 (7853), 248-252.

Wittmann, H., Oelze, M., Gaillardet, J., Garzanti, E., von Blanckenburg, F., 2020. A global rate of denudation from cosmogenic nuclides in the Earth's largest rivers. Earth-Science Reviews, 204, 103147.

Zeh, A., Gerdes, A., Klemd, R., Barton, J.M. 2007. Archaean to Proterozoic crustal evolution in the Central Zone of the Limpopo Belt (South Africa-Botswana): constraints from combined U-Pb and Lu-Hf Isotope analyses of zircon. Journal of Petrology, 48, 1605-1639.

Figure 1

Click here to access/download;Figure;Figure 1 Kalahari Erg.jpg

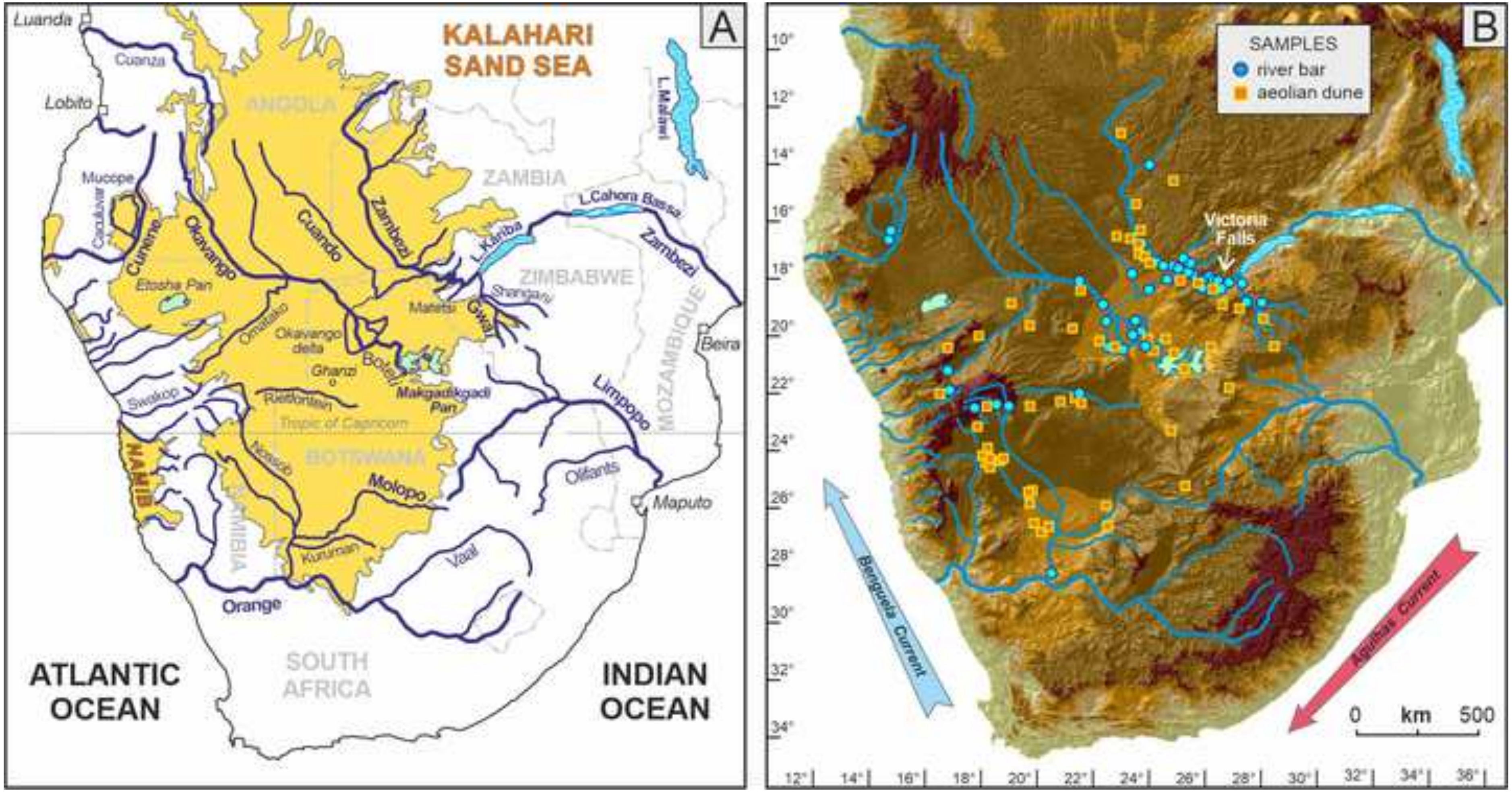

Figure 2

Click here to access/download;Figure;Figure 2 Kalahari Climate.jpg

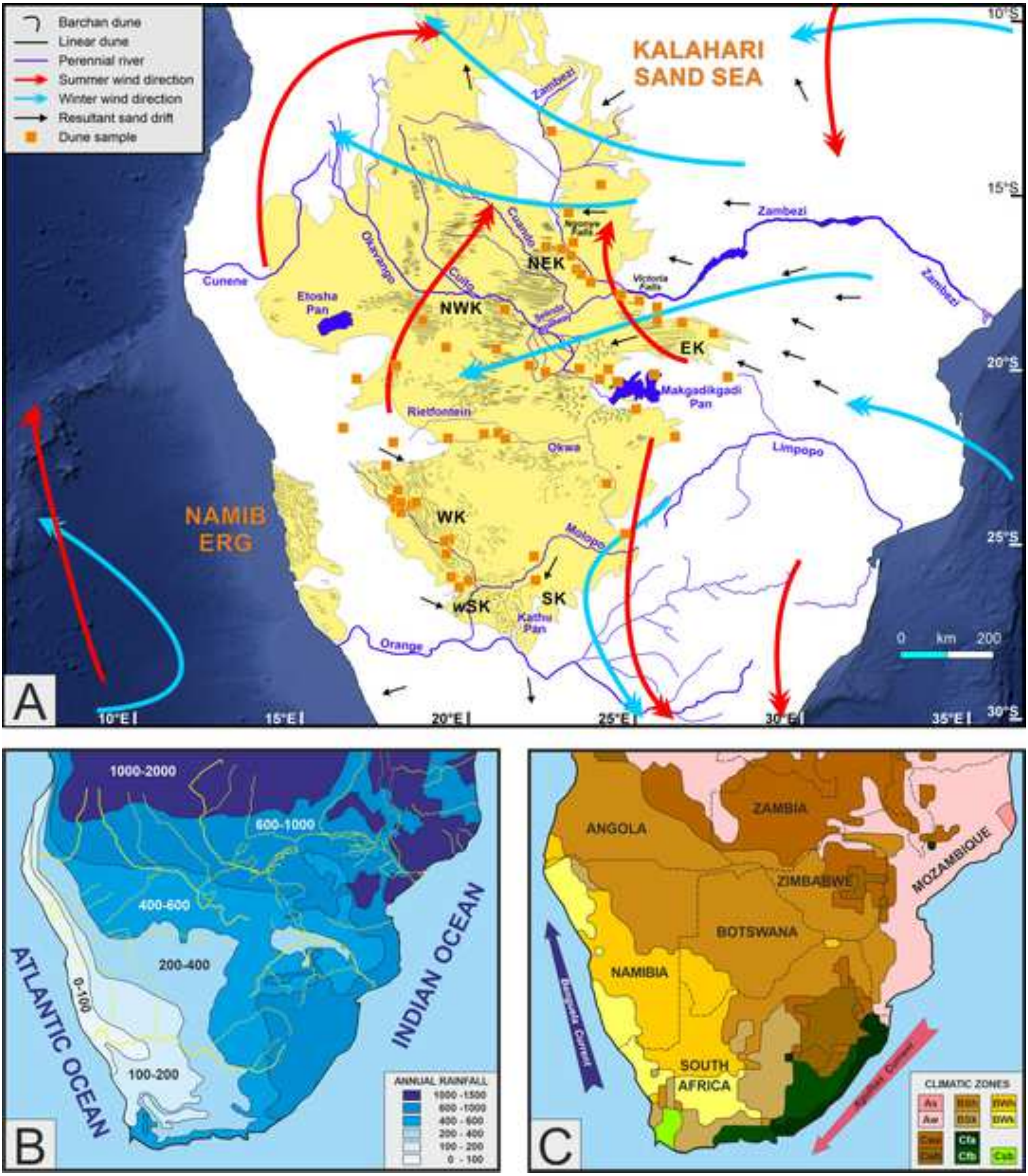

Figure 3 Click here to access/download;Figure;Figure 3 Kalahari Geology.jpg

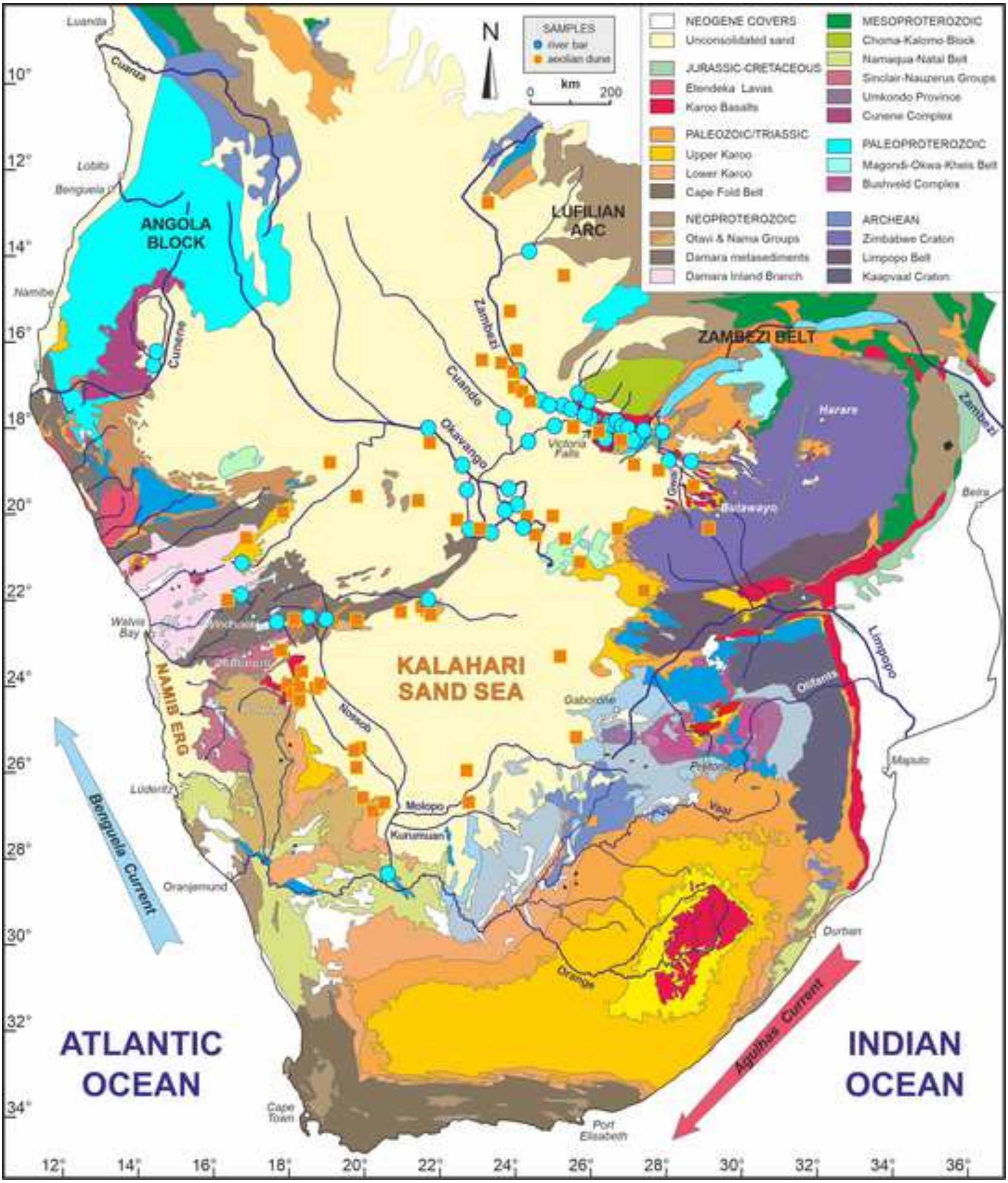

Figure 4a

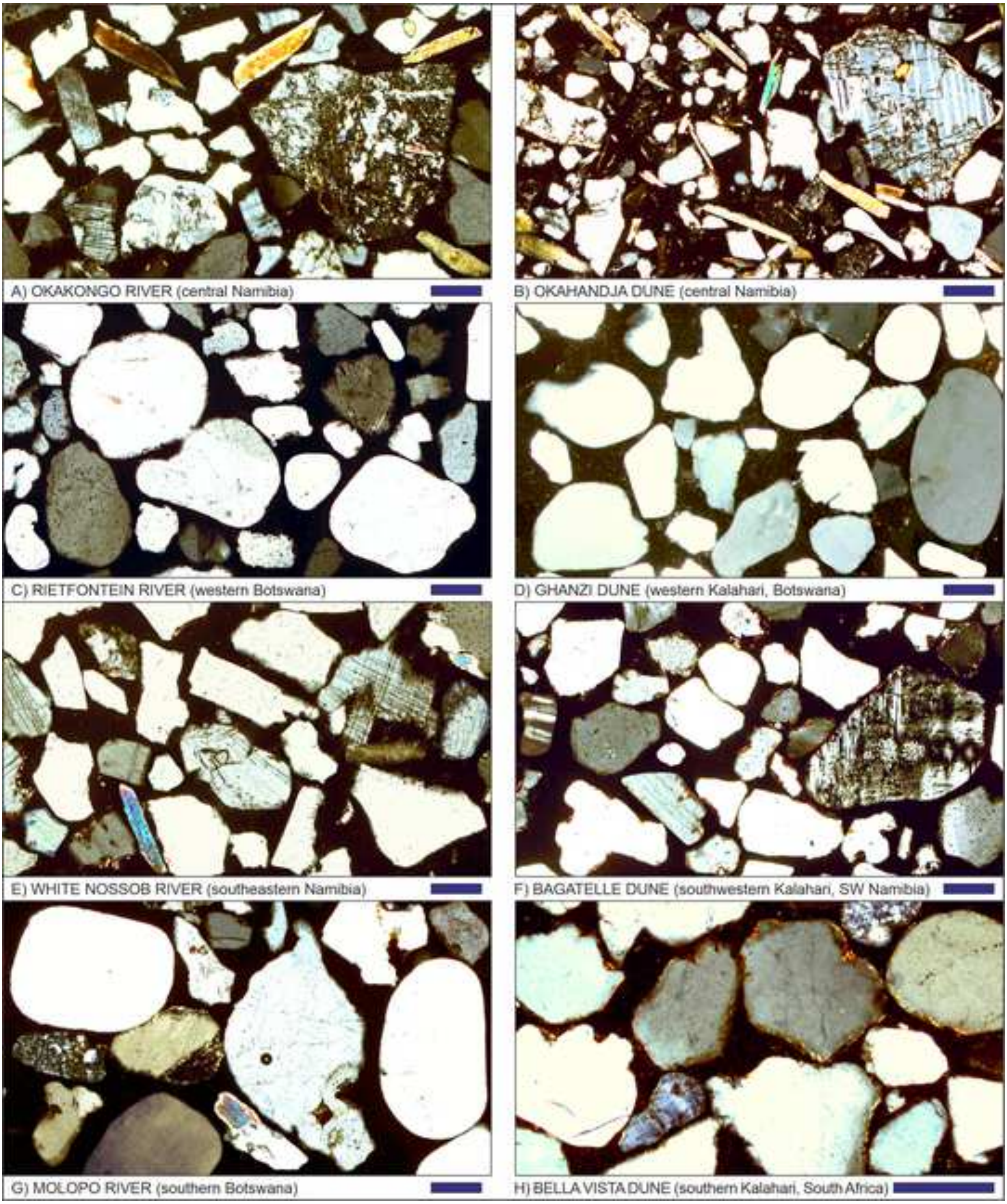
A) OKAKONGO RIVER (central Namibia)
B) OKAHANDJA DUNE (central Namibia)
C) RIETFONTEIN RIVER (western Botswana)
D) GHANZI DUNE (western Kalahari, Botswana)
E) WHITE NOSSOB RIVER (southeastern Namibia)
F) BAGATELLE DUNE (southwestern Kalahari, SW Namibia)
G) MOLOPO RIVER (southern Botswana)
H) BELLA VISTA DUNE (southern Kalahari, South Africa)

Figure 4b

Click here to access/download;Figure;Figure 4b Kalahari Foto East.jpg

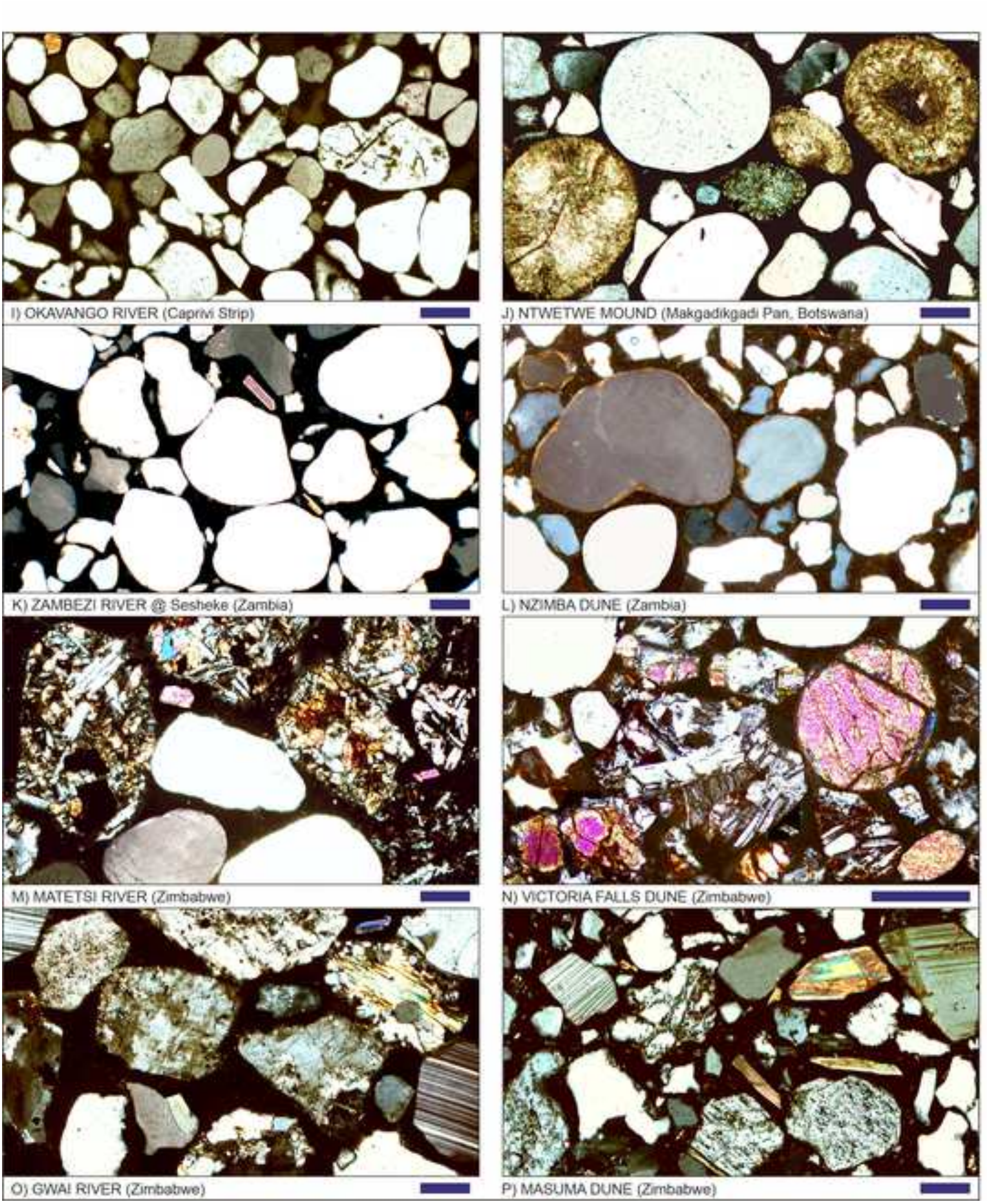

Figure 5 Click here to access/download;Figure;Figure 5 Kalahari QFL ZTR SKA AGE.jpg

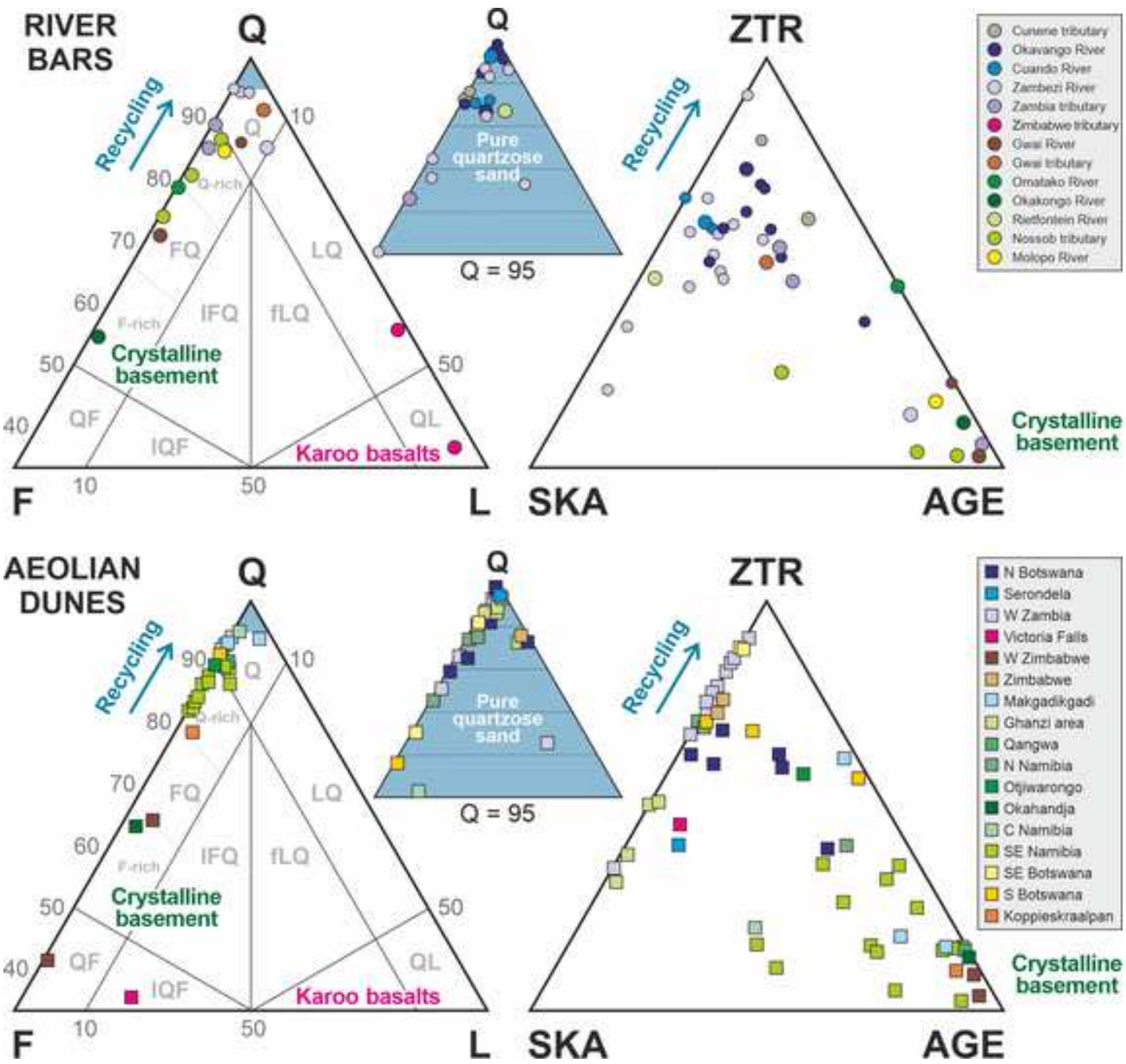

Figure 6

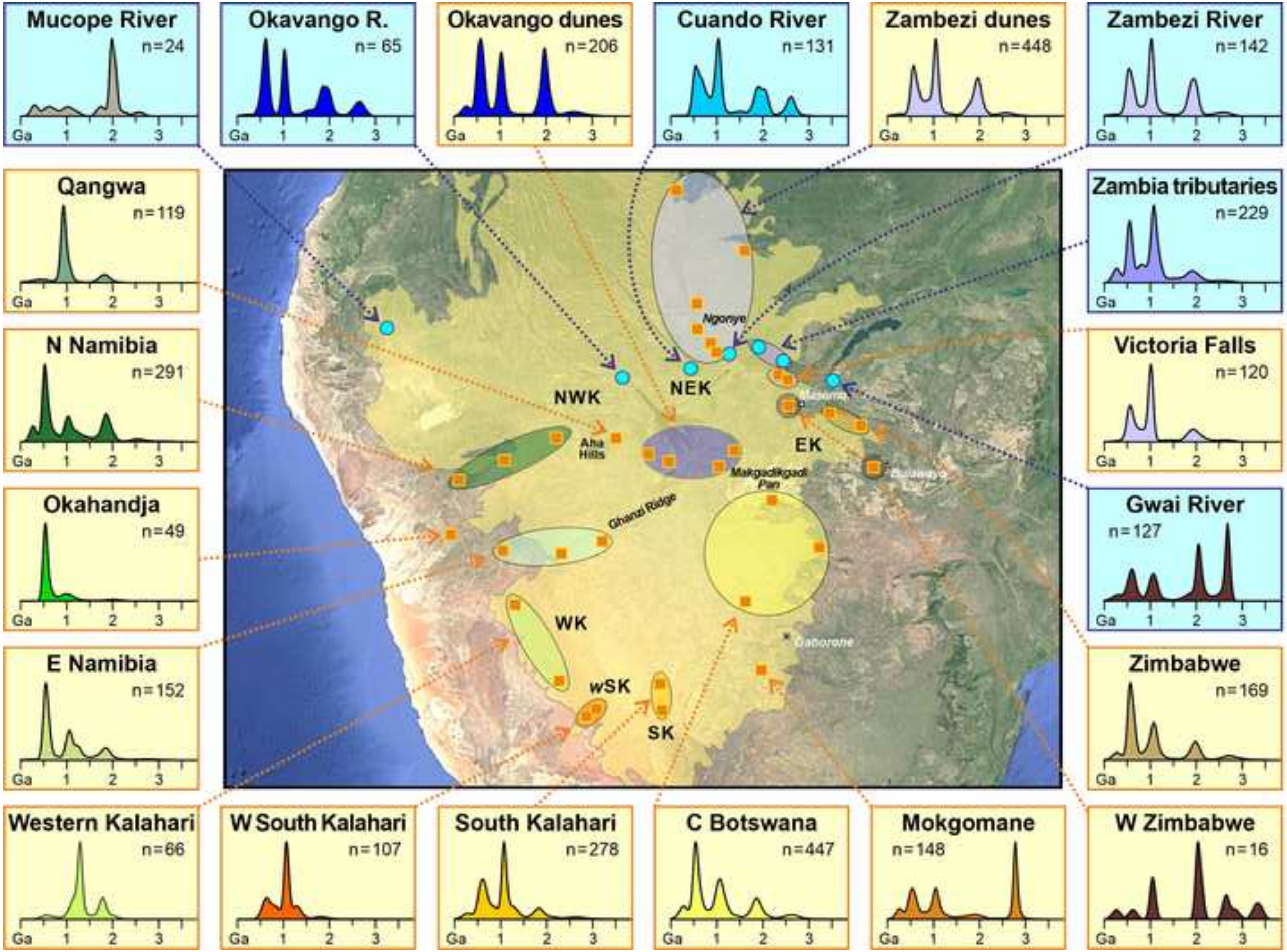

Mucope River
n=24
Okavango R.
n= 65
Okavango dunes
n=206
Cuando River
n=131
Zambezi dunes
n=448
Zambezi River
n=142
Qangwa
n=119
Zambia tributaries
n=229
N Namibia
n=291
Victoria Falls
n=120
Okahandja
n=49
Gwai River
n=127
E Namibia
n=152
Zimbabwe
n=169
Western Kalahari
n=66
W South Kalahari
n=107
South Kalahari
n=278
C Botswana
n=447
Mokgomane
n=148
W Zimbabwe
n=16
Ga
1
2
3
NWK
NEK
EK
WK
wSK
SK
Aha Hills
Ngonye
Ghanzi Ridge
Makgadikgadi Pan

Figure 7

Click here to access/download;Figure;Figure 7 Kalahari Zircon MDS.jpg

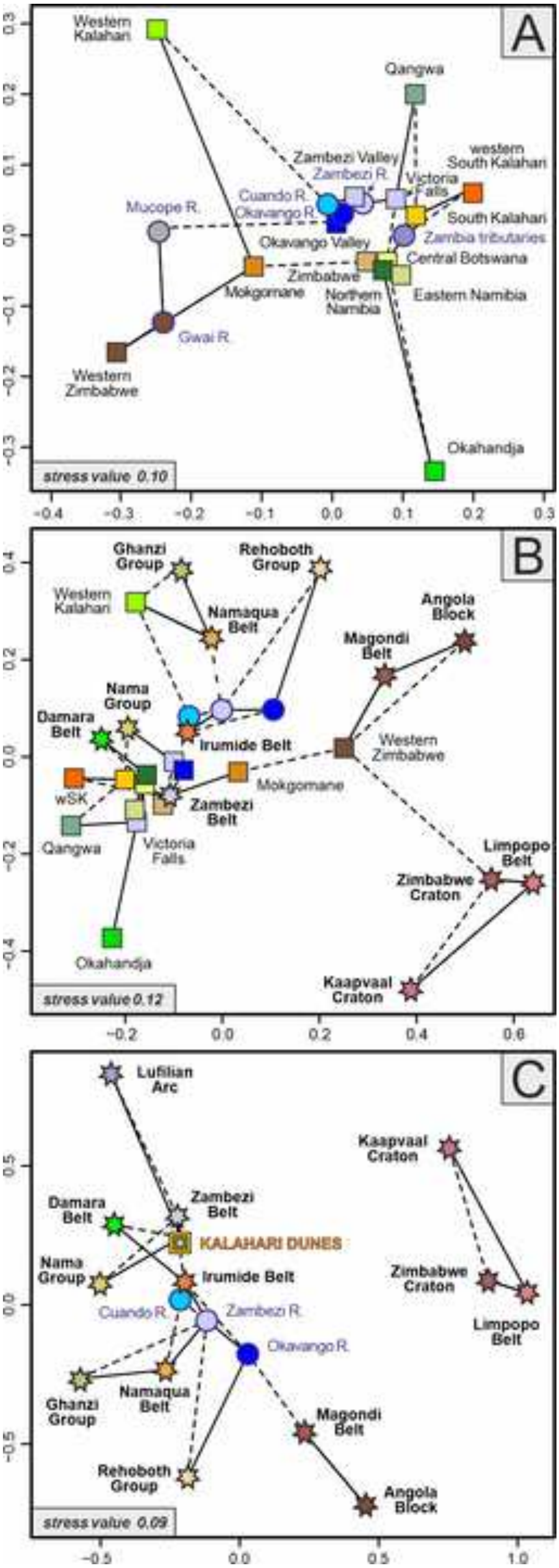

Figure 8

Click here to access/download;Figure;Figure 8 Kalahari dune Biplot .jpg

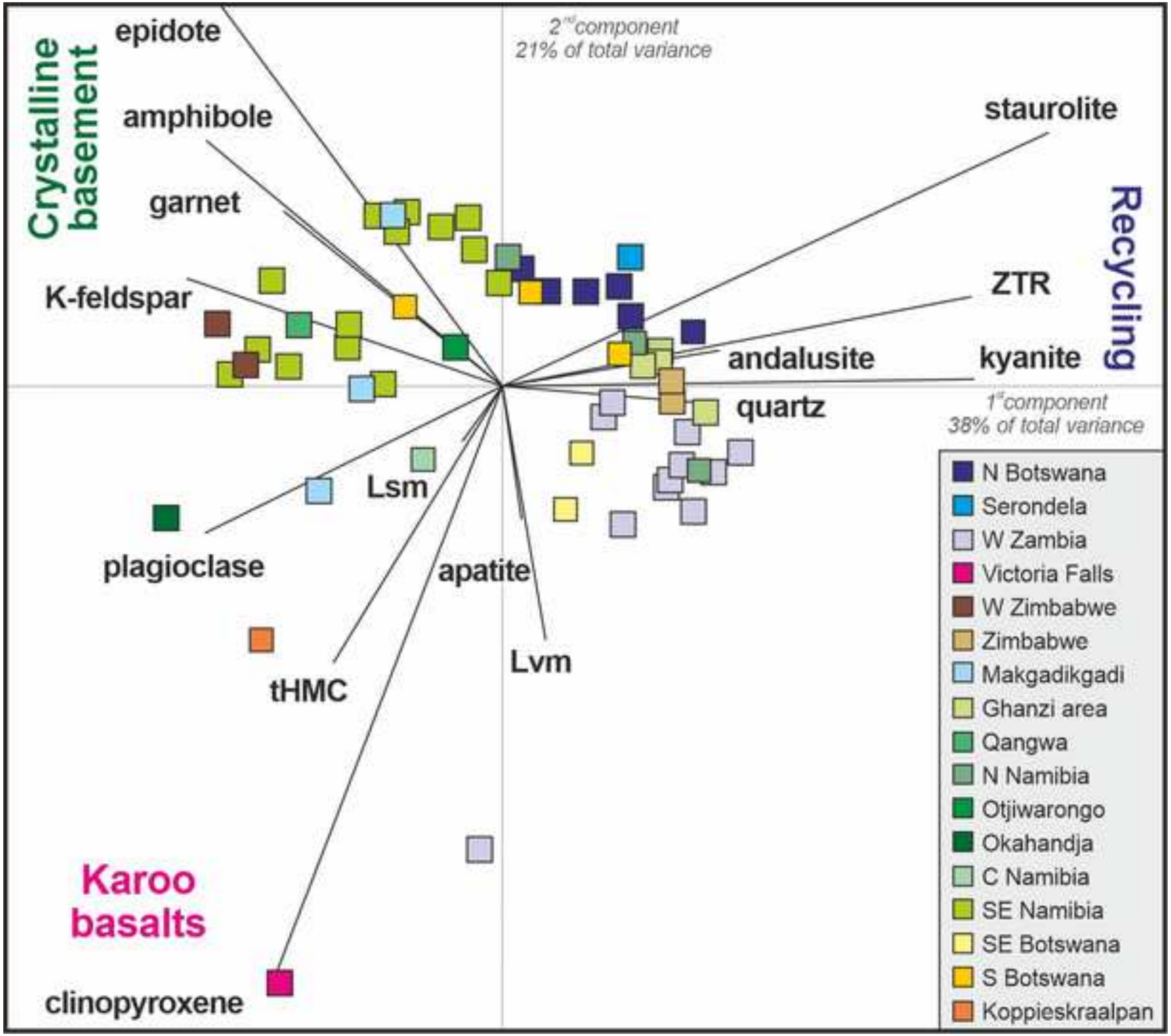

Figure 9

Click here to access/download;Figure;Figure 9 Kalahari PT HM Biplot .jpg

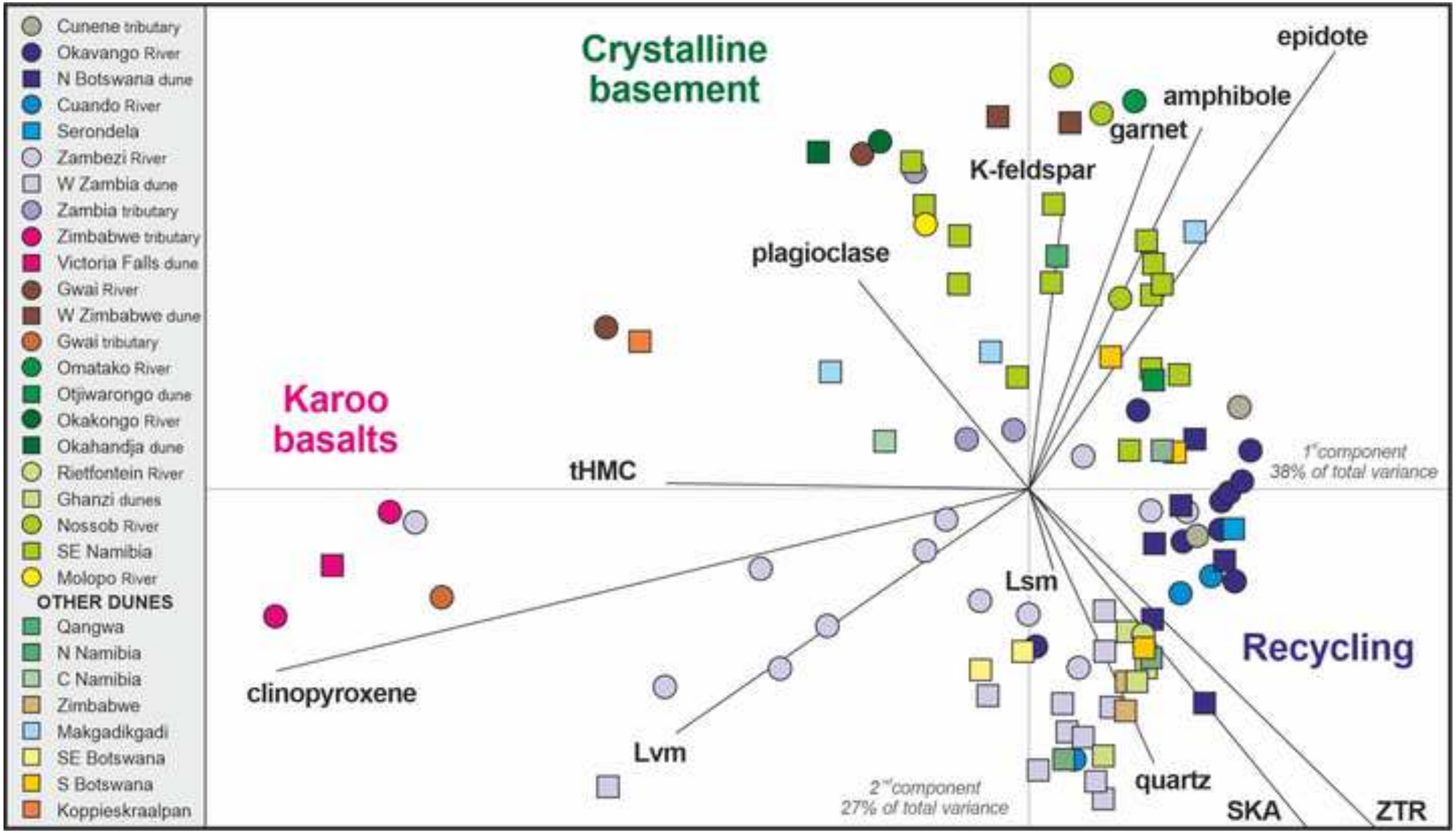

Figure 10

Click here to access/download;Figure;Figure 10 Kalahari Mineralogical Maps.jpg

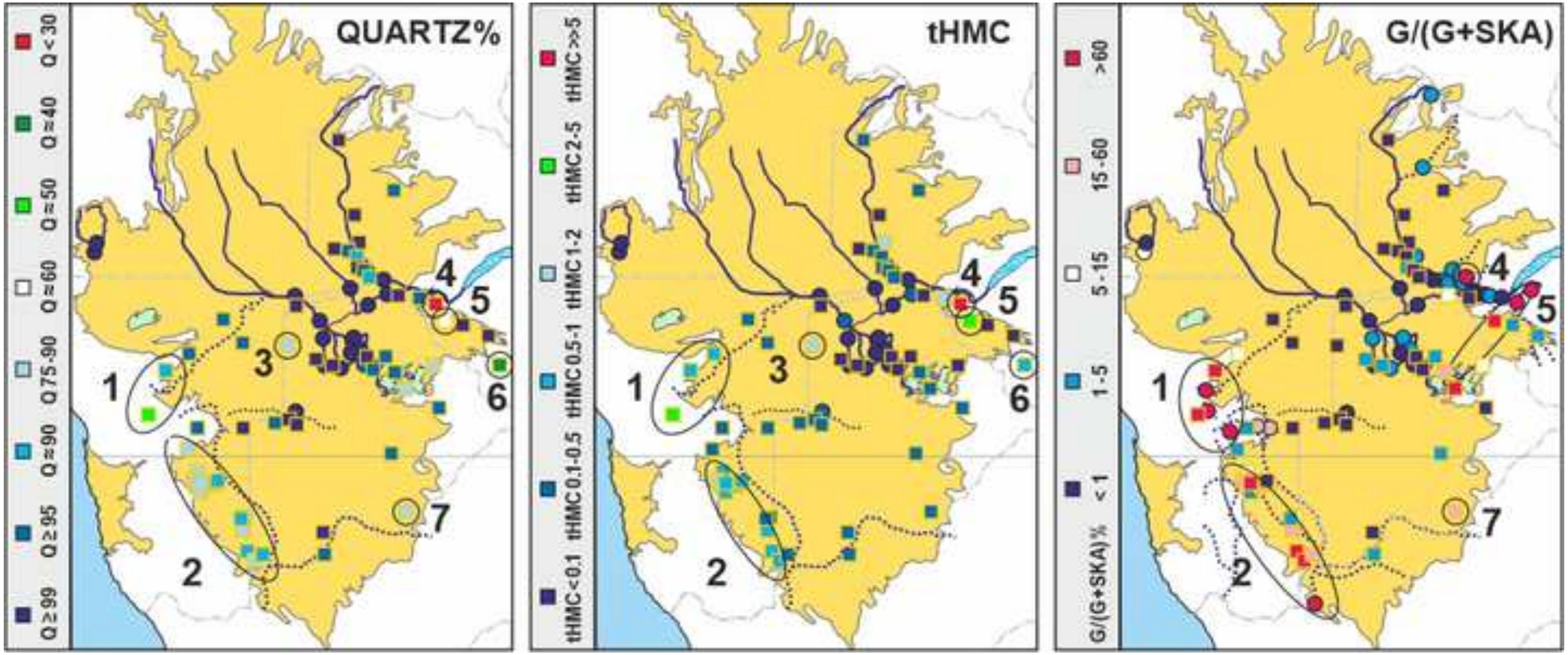

Table 1

	n°	Q	F	Lvm	Lsm		P/F%	MI*	tHMC	ZTR	Ap	Ep	Grt	St	Ky	Amp	Px	&tHM	
RIVERS																			
Cunene tributaries	2	99	1	0	0	100.0	13	n.d.	0.04	69	2	16	1	4	2	1	0	6	100.0
Okavango	9	99	0.5	0.1	0	100.0	n.d.	n.d.	0.06	57	0.4	15	0.3	14	6	5	0.2	2	100.0
Cuando	3	99	0.6	0.1	0	100.0	n.d.	n.d.	0.08	61	0.3	3	0	16	16	2	0	1	100.0
Upper.st Zambezi	7	97	3	0	0.1	100.0	32	n.d.	0.2	58	0.1	6	0.4	7	21	2	4	2	100.0
Upper Zambezi	1	85	5	9	0.3	100.0	50	n.d.	2.7	0	0.6	0	0	0	0	0.6	96	3	100.0
Matetsi	1	37	3	60	0.3	100.0	100	n.d.	33.3	0	0	0	0	0	0	0	100	0	100.0
Shangani	1	91	2	6	0	100.0	86	n.d.	4.7	1	0	0	0	0.5	0	0.5	98	0	100.0
Gwai	1	71	27	1	0.7	100.0	54	414	0.5	2	2	17	17	0	3	48	8	3	100.0
Omatako	1	79	21	0	0.3	100.0	21	n.d.	0.1	44	0	9	22	0	0	26	0	0	100.0
Okakongo	1	55	44	0	1	100.0	53	419	3.0	10	5	4	13	0.5	0	61	4	2	100.0
Rietfontein	1	98	0.7	0	1	100.0	n.d.	n.d.	0.2	46	0	1	0	43	8	3	0	0	100.0
Nossob	3	81	18	0	1	100.0	56	333	2.8	10	2	21	19	14	5	28	0	0.7	100.0
Molopo	1	85	11	0.3	4	100.0	69	200	0.9	14	2	28	14	4	2	28	8	0	100.0
DUNES																			
N Botswana	6	99	1	0.1	0.2	100.0	29	n.d.	0.1	58	1	16	0.3	16	7	1	0	1	100.0
Serondela	1	100	0	0	0.3	100.0	n.d.	n.d.	0.1	40	0	5	4	11	35	1	0	2.4	100.0
W Zambia	11	98	2	0.3	0	100.0	22	n.d.	0.4	72	0.3	0.1	0.1	10	10	0	7	0.2	100.0
Victoria Falls	1	35	49	15	0.4	100.0	99	n.d.	24.3	0.5	1	0	0	0	0.5	0	98	0	100.0
Masuma	1	64	32	0	4	100.0	71	296	3.0	3	5	24	64	0.5	2	1	0	0	100.0
Bulawayo	1	41	58	0	0.6	100.0	37	400	0.6	9	1	37	0	0	2	51	0	0.4	100.0
Zimbabwe	2	99	0	0.7	0	100.0	n.d.	n.d.	0.1	74	0.3	1	0.6	17	6	1	0	0.2	100.0
Makgadikgadi	3	93	6	0.6	0.2	100.0	25	143	0.2	28	0.6	40	2	2	4	8	13	2.1	100.0
Ghanzi area	4	99	0.4	0.1	0.3	100.0	n.d.	n.d.	0.2	43	0.2	1	0	48	7	0.5	0	0.3	100.0
N Namibia	3	98	2	0.1	0	100.0	0	n.d.	0.3	60	0	16	0.5	17	6	0	0	0.3	100.0
Qangwa	1	90	10	0	0	100.0	60	n.d.	1.6	15	3	78	0	1	0	2	0	0.5	100.0
Otjiwarongo	1	90	8	0	2	100.0	6	n.d.	0.7	55	1	3	24	1	11	1	0	3.9	100.0
Okahandja	1	63	34	0	2	100.0	60	367	3.0	11	9	7	2	0.5	0	60	10	0.5	100.0
C Namibia	1	95	4	1	0	100.0	21	n.d.	1.0	16	0.5	24	1	14	20	5	20	0	100.0
SE Namibia	14	86	13	0.4	0.5	100.0	10	250	0.7	18	0.3	54	4	12	3	5	2	0.6	100.0
SE Botswana	2	98	2	0	0	100.0	17	n.d.	0.1	87	0.2	0.7	0.2	9	1	0	1	0.2	100.0
Mokgomane	1	91	9	0	0	100.0	31	n.d.	0.3	57	0	40	1	0.5	1	0	0	0.5	100.0
S Botswana	2	97	3	0	0	100.0	43	n.d.	0.1	69	0.5	7	0.5	19	3	0.2	0	0.5	100.0
Koppieskraalpan	1	79	19	1	1	100.0	62	125	3.4	4	0	6	27	1	1	0	61	0.5	100.0

	peak 1	*frequency*	peak 2	*frequency*	peak 3	*frequency*	peak 4	*frequency*	peak 5	*frequency*
MODERN SANDS										
Cunene River	**1394 ± 5**	*28.6%*	**1746 ± 4**	*31.9%*	**1948 ± 4**	*36.7%*	**2456 ± 10**	*2.8%*		
Okavango River	**96 ± 1**	*2.1%*	**545 ± 2**	*23.8%*	**1040 ± 4**	*13.3%*	**1971 ± 2**	*49.6%*	**2607 ± 5**	*11.2%*
Cuando River	**29 ± 2**	*0.8%*	**590 ± 2**	*23.7%*	**1024 ± 3**	*30.9%*	**1902 ± 3**	*38.8%*	**2648 ± 6**	*5.8%*
Zambezi River	**646 ± 5**	*19.2%*	**1023 ± 6**	*27.4%*	**1193 ± 5**	*45.2%*	**2570 ± 8**	*8.2%*		
ANCIENT SANDSTONES										
Nama Group	**616 ± 1**	*20.8%*	**1010 ± 1**	*26.0%*	**1181 ± 1**	*38.3%*	**1891 ± 2**	*14.9%*		
Ghanzi Group	**1118 ± 1**	*50.3%*	**1259 ± 1**	*32.4%*	**1881 ± 1**	*17.3%*				
Rehoboth Group (Langberg and Billstein Fms.)	**1221 ± 2**	*22.5%*	**1858 ± 2**	*61.0%*	**2023 ± 3**	*16.5%*				
CRUSTAL DOMAINS										
Damara Belt (+ Cretaceous granite)	**131 ± 1**	*3.2%*	**523 ± 1**	*33.6%*	**794 ± 1**	*16.6%*	**1464 ± 1**	*35.8%*	**2096 ± 2**	*10.8%*
Lufilian Arc	**555 ± 1**	*41.6%*	**826 ± 1**	*43.1%*	**1125 ± 6**	*15.3%*				
Zambesi Belt	**485 ± 2**	*16.8%*	**827 ± 5**	*26.1%*	**1104 ± 1**	*34.1%*	**1794 ± 16**	*15.4%*	**2860 ± 4**	*8.0%*
Irumide Belt (+ Pan-African rejuvenation)	**597 ± 1**	*20.4%*	**1065 ± 1**	*28.7%*	**1140 ± 1**	*5.6%*	**1958 ± 1**	*27.7%*	**2354 ± 2**	*17.5%*
Namaqua Belt	**1119 ± 1**	*47.8%*	**1662 ± 1**	*30.3%*	**2003 ± 7**	*11.9%*	**23608 ± 1**	*9.9%*		
Magondi Belt (+ Pan-African rejuvenation)	**569 ± 7**	*7.1%*	**2080 ± 93**	*92.9%*						
Angola Block	**1935 ± 1**	*100.0%*								
Limpopo Belt (+ PPz tectono-thermal event)	**1953 ± 1**	*54.0%*	**2594 ± 1**	*29.1%*	**3284 ± 2**	*16.9%*				
Zimbabwe Craton (+ PPz tectono-thermal event)	**1881 ± 1**	*11.7%*	**2411 ± 1**	*44.8%*	**2580 ± 1**	*43.6%*				
Kaapvaal Craton (+ Vredefort magmatic rocks)	**977 ± 4**	*8.8%*	**2845 ± 1**	*7.3%*	**3467 ± 2**	*83.9%*				